(12) LEVEL II

DNA 4481F

BLAST AND THERMAL EFFECTS OF MULTIPLE NUCLEAR BURST EXPOSURE OF AIRCRAFT IN A BASE-ESCAPE MODE

Kaman AviDyne
83 Second Avenue
Burlington, Massachusetts 01803

October 1977

Final Report for Period January 1977 — October 1977

CONTRACT No. DNA 001-77-C-0053

THIS WORK SPONSORED BY THE DEFENSE NUCLEAR AGENCY
UNDER RDT&E RMSS CODE B342077464 N99QAXAE50604 H2590D.

Prepared for
Director
DEFENSE NUCLEAR AGENCY
Washington, D. C. 20305

Destroy this report when it is no longer needed. Do not return to sender.

UNCLASSIFIED

SECURITY CLASSIFICATION OF THIS PAGE (When Data Entered)

REPORT DOCUMENTATION PAGE	READ INSTRUCTIONS BEFORE COMPLETING FORM
1. REPORT NUMBER DNA 4481F	2. GOVT ACCESSION NO. / 3. RECIPIENT'S CATALOG NUMBER
4. TITLE (and Subtitle) BLAST AND THERMAL EFFECTS OF MULTIPLE NUCLEAR BURST EXPOSURE OF AIRCRAFT IN A BASE-ESCAPE MODE	5. TYPE OF REPORT & PERIOD COVERED Final Report [redacted] Jan [redacted]—Oct [redacted]77
	6. PERFORMING ORG. REPORT NUMBER KA-TR-146
7. AUTHOR(s) Raffi P. Yeghiayan William N. Lee John P. Walsh	8. CONTRACT OR GRANT NUMBER(s) DNA 001-77-C-0053
9. PERFORMING ORGANIZATION NAME AND ADDRESS Kaman AviDyne 83 Second Avenue Burlington, Massachusetts 01803	10. PROGRAM ELEMENT, PROJECT, TASK AREA & WORK UNIT NUMBERS NWED Subtask N99QAXAE506-04
11. CONTROLLING OFFICE NAME AND ADDRESS Director Defense Nuclear Agency Washington, D.C. 20305	12. REPORT DATE Oct [redacted]77 13. NUMBER OF PAGES 76
14. MONITORING AGENCY NAME & ADDRESS(if different from Controlling Office)	15. SECURITY CLASS (of this report) UNCLASSIFIED 15a. DECLASSIFICATION/DOWNGRADING SCHEDULE

16. DISTRIBUTION STATEMENT (of this Report)

Approved for public release; distribution unlimited.

17. DISTRIBUTION STATEMENT (of the abstract entered in Block 20, if different from Report)

18. SUPPLEMENTARY NOTES

This work sponsored by the Defense Nuclear Agency under RDT&E RMSS Code B342077464 N99QAXAE50604 H2590D.

19. KEY WORDS (Continue on reverse side if necessary and identify by block number)

Multiple Nuclear Burst Effects
Blast Gust Response
Blast Overpressure Response
Thermal Response
Structural Dynamics
Aircraft Vulnerability
Base Escape

20. ABSTRACT (Continue on reverse side if necessary and identify by block number)

Analytical methods are employed to investigate the enhancement or attenuation of gust, overpressure, and thermal radiation effects due to multiple nuclear bursts in comparison with worst-case single burst exposure. The nuclear attack scenario assumes placement of the simultaneous nuclear bursts in a low-altitude planar hexagonal close-packed configuration to damage aircraft in a base-escape mode. Symmetry considerations are taken into account in investigating the possible aircraft position and flight path orientations.

DD FORM 1 JAN 73 1473 EDITION OF 1 NOV 65 IS OBSOLETE

78 07 [redacted] 08

UNCLASSIFIED

SECURITY CLASSIFICATION OF THIS PAGE (When Data Entered)

PREFACE

This report was prepared for the Defense Nuclear Agency under Contract No. DNA001-77-C-0053. The analytical work was carried out in the Structures Group at Kaman AviDyne under the supervision of Mr. Emanuel S. Criscione. Major David Garrison and Capt. Michael Rafferty were the DNA Contracting Officer's Representatives. Their guidance and assistance, as well as contributions from the technical staff at Kaman AviDyne are deeply appreciated. Acknowledgement is particularly due to Dr. Norman P. Hobbs, Technical Director, for his many suggestions and to Lawrence J. Mente for his study of overpressure damage to panels and stringers.

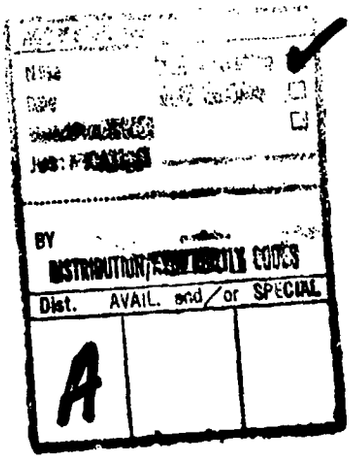

TABLE OF CONTENTS

LIST OF ILLUSTRATIONS

LIST OF ILLUSTRATIONS (CONTINUED)

LIST OF TABLES

SECTION I
INTRODUCTION

The effects of nuclear-weapon-generated blast and thermal radiation environments on aircraft have been and continue to be of major interest in military planning. Many problems associated with these environments have been under study, such as the response of in-flight aircraft structures subjected to a single nuclear burst environment. Some related response problem areas have not been adequately investigated and require study to better understand the overall vulnerability of an aircraft weapon system. One such problem area is the response of aircraft subjected to the blast and thermal radiation generated by multiple nuclear bursts.

This report presents the results of an analytical study of one aspect of the multiple exposure problem: the gust, overpressure, and thermal radiation effects due to multiple nuclear burst exposure of aircraft in a base escape mode. One of the war gaming scenarios of current interest in assessing aircraft survivability is an aircraft base under a submarine-launched ballistic missile attack, with the aircraft attempting to escape. This gives rise to a situation where escaping aircraft may simultaneously be exposed to the blast and thermal radiation fields generated from multiple nuclear weapons. Different geometric burst patterns and burst timing sequences need to be examined to determine the worst possible configurations affecting aircraft survivability. Combinations where enhancement effects either from blast or thermal radiation due to multiple bursts become significant will have an important bearing in the assessment of the survivability of aircraft. Consequently, the objective of the current study is to compare the survivability of aircraft for multiple exposures with the survivability for the worst single-burst condition.

Kaman AviDyne has previously examined the blast field within the overlapping lens region of two bursts in a study of missile vulnerability and has carried out a comparison of the multiple burst environments from various computer codes (Refs. 1 and 2). The vulnerability study of missiles subjected to multiple bursts has identified certain traversal

orientations producing significant enhancement. With the above background, an exploratory study was carried out to investigate the multiple nuclear blast exposure effects on aircraft in a base escape mode. The methods of analysis and the results obtained are presented in the following sections. Section II presents the geometric "laydown" pattern of the multiple burst centers selected for the study and discusses the considerations entering into the selection of the configurations. Section III describes the analysis method and presents the results of the multiple burst environment studied. Section IV presents the analysis and results of the gust environment, and Section V presents the analysis and results of the overpressure environment. The thermal radiation environment and the coupled thermal/overpressure environment due to multiple nuclear bursts are presented and discussed in Sections VI and VII. Finally, the conclusions and recommendations for further study are presented in Section VIII.

SECTION II
MULTIPLE BURST LAYDOWN PATTERN

In a study of the vulnerability of aircraft exposed to multiple nuclear bursts an infinite number of configurations are possible with variations in the number of the nuclear bursts, the locations of the burst centers in three-dimensional space, the timing sequence of the bursts, and the aircraft flight path orientations and altitude. It is obvious that for an exploratory study many simplifying assumptions and limitations of scope need to be made to reduce the problem to a manageable size.

The information provided in Ref. 3 was used as a basis for limiting the number of burst configurations to be addressed. The scenario of interest is a strategic aircraft base under attack by submarine-launched ballistic missiles. The aircraft will be taking off and climbing out as rapidly as possible. Figure 1 depicts a hypothetical situation with five nuclear bursts defining a sure-safe and sure-kill envelope for the scrambling aircraft. Assuming that the attacking enemy can carefully control the burst center location and timing, and in view of the fact that the escaping aircraft will be in random positions and orientations, the attacker would deliver all warheads for simultaneous arrival and burst (to minimize the advance notice time) and would choose a laydown pattern that would equally distribute the critical destructive power over the largest area possible. It is thus assumed that the laydown pattern would be a hexagonal close-packed configuration in one horizontal plane, as shown in Figures 2 and 3. Figure 2 shows the configuration with the shock fronts just prior to overlap, and Fig. 3 shows the overlapping shock fronts forming the lenticular interaction regions. The distance between burst centers would be governed by the assumed hardness level of the aircraft under attack, since the lethal radius of each burst will decrease with increasing hardness of the structure under attack.

For further simplification, the plane defined by the burst centers was selected to be the zero altitude, sea-level plane. Thus, hemispherical shock fronts are generated, and ground reflection is accounted for as a mirror-image, without the co plications of a complex geometry that would result when bursts at altitude intercept the ground plane.

Limiting the flight path of the aircraft to the same sea-level plane of the burst centers, symmetry considerations reduce the blast environment to be studied to a 30-degree sector of a centrally-located burst. Since aircraft flight direction is arbitrary in this plane, flight paths initiating within a grid of the 30-degree sector and aiming in various compass directions will adequately represent the possible intercept configurations. Figure 4 shows a hexagonal close-packed laydown pattern of seven simultaneous bursts and the 30-degree segment for symmetry. By reflective symmetry about the zero-degree boundary one obtains the information pertinent to the remaining 30-degree sector of a peripheral burst interacting with the central burst, and the combined 60-degree sector is repeated for the remaining five peripheral bursts.

The attack scenario employed for the gust and overpressure environment study consisted of seven simultaneous bursts of one megaton yield each, laid down at sea level in the hexagonal close-packed configuration discussed earlier. The bursts were positioned such that at least a two psi overpressure level would be encountered by the intercepted aircraft. This two psi overpressure level was selected in view of the hardness of representative aircraft to blast overpressure damage. The overpressure requirement resulted in burst center separations of 52,000 feet, based on blast radii of approximately 30,000 feet, overlapping as shown in Figure 3. Wi in the 30-degree sector for symmetry, nine aircraft start points were selected, with aircraft flight path headings at 30-degree intervals from each start point. Again, due to symmetry, not every heading had to be analyzed at start points on the boundaries. Figure 5 shows the selected aircraft positions and flight path orientations at first blast intercept for this study. Aircraft positions closer to the central burst need not be considered since, for such positions, the

blast/thermal environment from other bursts is very small in comparison with the blast/thermal environment from the central burst.

For the thermal radiation environment study, in addition to the simultaneous bursts in a hexagonal configuration around a center burst, a hexagonal close-packed laydown of nineteen simultaneous bursts, as shown in Figure 3, was also studied. Also, a non-simultaneous burst hexagonal close-packed laydown pattern was considered for the thermal/overpressure coupling effects.

SECTION III
BLAST ENVIRONMENT

3.1 Introduction

The initial effort in the study of multiple nuclear blast-induced gust and overpressure effects on aircraft was aimed at studying the environment generated by the multiple nuclear blasts. Following a preliminary investigation of available codes and their features, the LAMB (Low Altitude Multiple Burst) code was selected for the study of the environment (Ref. 4). An updated version of LAMB VI was obtained on magnetic tape and employed for this study.

A single burst of 1 megaton yield, occurring at zero altitude (ground level) and incorporating ground reflection, was employed to generate overpressure levels versus range from the burst center. The results are shown in Figure 6. Based on the hardness of representative aircraft to blast overpressure damage, a minimum of two psi overpressure level was selected as a requirement for the blast-generated environment - a plausible objective in the attack scenario. As seen in Figure 6, for the 1 MT LAMB-generated environment, including ground reflection, blast radii smaller than 30,000 ft. produce overpressure levels larger than two psi. A hexagonal close-packed laydown pattern for multiple bursts, such that the whole area is covered with at least the required two psi overpressure level, results in burst center separations of 52,000 ft., as shown in Figure 3 and detailed in Figure 5. Also shown in Figure 5 are the nine positions of the aircraft within the 30° segment for symmetry, discussed in Section II. The nine positions represent the aircraft locations at the time of first (closest) blast arrival. From that instant on, the aircraft are assumed to be flying in a straight flight path oriented in the headings shown at 30-degree intervals.

Figure 7 shows the LAMB 1 MT blast radius versus time after burst. Superposed on the curve are the tick marks indicating the blast radii at intercept with the nine aircraft positions, and the associated times of arrival. The information is tabulated as an inset in the figure. Thus, the aircraft position closest to the burst center (position 7) at a distance of 20,000 ft. from the burst center is intercepted 11.97 sec. after the burst, and the aircraft position farthest from the burst center (position 3) at a distance of 30,022 ft. from the burst center is intercepted 20.45 sec. after the burst.

The study of the environment impinging on the aircraft was carried out by exercising the LAMB code with the blast front just ahead of intercept with a selected aircraft position, and calculating the environment for a point advancing at the speed of the aircraft in a selected heading. Aircraft speed was specified to be 525.0 ft./sec. Due to symmetry considerations, not all of the headings from each position had to be investigated at the boundaries of the 30-degree segment for symmetry; the arrows shown in Figure 5 indicate the headings employed. A total of 66 combinations of position and heading were studied.

3.2 Presentation of Results

As visual aids to understanding the environment generated by the interacting shock fronts from the multiple blasts, graphic displays and machine plots were generated to show overpressure and density contours; material velocity flow fields; time histories of overpressure, density, and material velocity at specific points in space; and time histories of the material velocity normal to specified flight paths. Figures 8(a) through 8(c) depict representative plots of overpressure and density contours, and material velocity vectors for two interacting bursts generated in the preliminary phase of this study. Figures 9(a) through 9(c) depict representative time histories of the side gust (material velocity normal to flight path), overpressure, and density for the aircraft following the flight path at a heading of 150° from position 4 (see Figure 5). The first discontinuity indicates the arrival of the first shock, and subsequent discontinuities indicate the arrivals of the other

interacting shock fronts. It should be noted that the side gust plot of Figure 9(a) represents a component of the velocity vector (the component normal to the flight path) and the magnitudes depend on the orientation of the flight path relative to the burst centers. Thus, the side gust from the closest burst may be smaller in magnitude than that caused by a burst further away but impinging at a larger angle to the flight path, as is the case in the figure shown. The extreme case, of course, would be a heading aiming at the center of the closest burst, which would cause no normal velocity component or side gust on the aircraft. However, the overpressure and density jumps, as seen in Figures 9(b) and 9(c), decrease with each subsequent shock arrival. Not only do the jumps decrease, but the largest overpressure and density are associated with the first shock arrival, with subsequent peaks being smaller. This results from the long time separation between shock arrivals, allowing earlier blast waves to have decayed prior to subsequent shock arrivals. Only when arrival times are very close, such that the magnitudes from earlier blasts have not decayed, will there be an enhancement of overpressure or density.

Side gust, overpressure, and density results were similarly obtained for all 66 combinations of aircraft position/flight path orientation. Maximum values for all three quantities were noted in the analysis of the results. Pertinent results are presented and discussed in the following sections of this report.

SECTION IV
GUST EFFECTS

4.1 Introduction

The attack scenario and laydown pattern of multiple nuclear bursts, as well as the environment generated by the bursts, have been discussed in earlier sections. This section details the results of the study of gust effects on aircraft intercepted by the nuclear bursts.

Since aircraft response to side gusts is of concern, the material velocity generated by the nuclear bursts was employed to calculate the side gust, or component perpendicular to the flight path. The flight path analysis program was used to analyze the side gust environment from LAMB VI for the multiple bursts, as well as from a single "critical burst" (the one that generates the greatest gust normal to the flight path) for all combinations of aircraft location and flight path orientation. Again, the objective is to compare the multi-burst environment with the worst single burst environment.

As discussed earlier, the multiple burst gust environment is generated by seven simultaneous bursts placed in a hexagonal close-packed laydown pattern with burst center separations of 52,000 ft. Nine aircraft starting positions within a 30-degree segment and selected headings at 30-degree intervals were used, as shown in Figure 5. By symmetry, the results obtained from the selected 30-degree segment apply to the remaining segments of the seven-burst laydown pattern.

4.2 Results of Analysis

Having defined the side gust environment acting on the aircraft, one needs to consider the structural system that will respond to the forces generated by that environment. Since the scope of this study was limited to investigating possible enhancement or attenuation in the response of aircraft subjected to multiple bursts in comparison with the effects of a single burst, a simple one-degree-of-freedom system was selected to study the response. Two natural frequencies were considered for the responding system, 1 Hz and 5 Hz, representative

response frequencies for aircraft that may be subject to the attack scenario. Damping values of 5 and 10% of critical damping were employed in generating response runs for this simple system. Since the results were very similar, only the 5% damping results are presented.

Figure 9(a) shows a representative side gust time history and pertains to an aircraft at location 4 and heading in the 150° direction in the seven simultaneous bursts laydown pattern. For the same aircraft flight path, Figure 10 shows the side gust time history for the single "critical burst" located, in this case, at the center of the hexagonal close-packed seven burst pattern. Since no other shock fronts are considered the secondary discontinuities in side gust (seen in Figure 9(a)) are not present.

Similar results were obtained for all 66 aircraft location and orientation combinations within the 30° segment of symmetry. The absolute values of the peak side gusts and the times at which they occur are tabulated for all cases investigated in the first three columns of Tables 1 and 2. Table 1 shows the results for the seven simultaneous bursts configuration, and Table 2 shows the results for the selected single critical burst. The first column in each table identifies the case under investigation, by giving the aircraft location number and the flight path orientation angle in degrees, as seen in Figure 5, for the 66 test cases. The peak side gusts (absolute values, ft/sec) are tabulated in the second column, and the time (sec) at which they occur is tabulated in the third column (t=0 is the burst time).

Representative time histories of the one-degree-of-freedom aircraft response are shown in Figure 11 for the seven simultaneous burst case, and in Figure 12 for the selected single "critical burst" case for position 4 and orientation 150°. Figures 11(a) and 12(a) show the displacement, Figures 11(b) and 12(b) show the velocity, and Figures 11(c) and 12(c) shows the acceleration for the 1 Hz natural frequency case with 5% damping imposed.

Similar results were obtained for all 66 cases investigated with 1 Hz or 5 Hz natural frequencies. The maximum displacements and the times when they occur are tabulated in the last four columns of Tables 1 and

2, for the multiple and the single burst cases, respectively. Results are shown for the 1 Hz and the 5 Hz response cases with 5% damping imposed.

Table 3 uses the data shown in Tables 1 and 2 for a comparison of the side gust environment and displacement response as a ratio of the effects of the multiple vs. single burst cases investigated. It should be noted that values above unity represent enhancement of effects when multiple simultaneous bursts occur, and values below unity represent attenuation when multiple simultaneous bursts occur. Note that enhancement, where present, is very small in magnitude, and occurs at only a few of the position/orientation configurations investigated.

The peak displacement ratio information shown in Table 3 is shown graphically in Figure 13(a) for the 1 Hz response, and in Figure 13(b) for the 5 Hz response cases. A magnified section of the 30-degree segment of symmetry is shown, indicating the nine aircraft starting positions in the cartesian coordinate system of Figure 5. For each aircraft starting position, the envelope for the peak displacement of the one-degree-of-freedom system as a function of flight path angle is shown with the scale indicated. The solid lines represent the magnitudes of the peak displacements in response to the single critical burst, and the dashed lines represent the response to the seven simultaneous bursts. It becomes obvious that gust effects enhancement due to multiple exposures occurs in very limited cases and is small in magnitude. Definite attenuation occurs at the boundaries of the segment for symmetry. This is due to the cancellation effect of the side gusts arriving from opposite directions simultaneously due to symmetrically-placed simultaneous bursts. The attenuation would be strongly affected if the blasts were not simultaneous, such that the side gust arriving from one direction would precede the lagging side gust from the opposite direction.

SECTION V
OVERPRESSURE EFFECTS

5.1 Introduction

The attack scenario and laydown pattern of multiple nuclear bursts, as well as the environment generated by the bursts, have been discussed in earlier sections of this report. This section details the results of the limited study of overpressure effects on aircraft intercepted by the nuclear bursts.

The multiple burst overpressure environment is generated by seven simultaneous bursts placed in a hexagonal close-packed laydown pattern in the zero altitude ground plane. Intercepted aircraft are also considered to be flying in the plane defined by the burst centers. In this flight configuration, overpressure effects would have the greatest effect on planar surfaces perpendicular to the plane of the bursts. An aircraft flying towards the center of a burst would offer relatively small planar surfaces perpendicular to the plane of the bursts. However, an aircraft flying in a tangential direction relative to the burst sphere would have the relatively large planar surfaces of the vertical fin exposed to the laterally impinging blast wave. Hence, damage to the vertical tail is selected for the study of multiple exposure vulnerability to blast overpressure.

Two situations are of primary interest for multiple exposure overpressure effects. The first of these is for point 1 in Figure 5, for which the blast waves from two bursts arrive simultaneously but from opposite sides. In this case the loading is similar to a single blast wave reflecting off a wall of infinite extent, in which case the clearing time is infinite. The fact that clearing does not take place leads to the possibility that overpressure damage will be significantly enhanced with respect to the single burst case.

The second situation of interest is sequential loading of a structure. If the first loading produces damage (inelastic response), can the damage be enhanced by subsequent loading from a multiple burst environment?

5.2 Panel and Stringer Damage From Simultaneous Blast Waves

For structural response to overpressure from simultaneous blast waves from opposite sides, the response enhancement of a multiple-burst pattern relative to a single burst is demonstrated using a structural panel and stringer from the vertical fin of a representative aircraft. The aluminum panel is 8 in. by 24 in. and .032 in. thick. The stringer used is a 42 in. long hat section. The loading considered is for a multiple burst condition defined by LAMB which gave a peak pressure of 5.1 psi and a decay to zero in 3.75 seconds. The response characteristics of these structures are such that this loading is practically a step input over the response time of interest. To simulate a single burst loading for comparison, clearing times for the reflected pressure of 5.1 psi are assumed based on distances from the leading edge of the fin of 2, 6 and 12 feet. Table 4 shows the response comparison for the flat panel and stringer in terms of maximum deflections and strains. For the flat panel the differences in response between single and multiple burst loadings are less than 10% and are not considered significant. For the stringer the differences can be significant if the stringer is located near the leading edge, but for locations in the interior of the fin the differences are not considered significant. It should be noted that the differences shown in Table 4 would be somewhat smaller if presented in terms of a slant range comparison.

5.3 Cumulative Damage Due to Sequential Overpressure Exposure

Due to the relatively small enhancement noticed when comparing overpressure effects due to multiple bursts versus a single burst, it was decided to carry out a limited study of a plausible worst-case sequential exposure situation. In this situation, it is stipulated that the overpressure effect of the first blast is to cause strains beyond the elastic limit for a representative panel, such that a set deformed shape is obtained after the effects of the first blast subside. The arrival of an identical overpressure due to the second blast in the sequence is then applied to the deformed shape to determine whether significant further damage (additional permanent strain) can be imposed.

For this study a beam element model, simulating a strip from the rectangular panel of the vertical fin employed in the earlier study, was chosen. The thickness of the panel and the applied overpressure magnitude were scaled down to eliminate bending strain considerations; thus the very thin panel was essentially subjected to just membrane strains. The beam was of unit width, 8.5 in. long, pinned at the ends. The thickness employed was 0.00004 in., and material properties of 2024-T3 were used. A bi-linear stress-strain curve, shown in Figure 14, was used.

The applied overpressure was a triangular pulse with 0.05 psi peak overpressure decaying linearly to zero in 5.0 seconds. A modified version of the NOVA program, NOVA-2L, was employed (Reference 5). The results obtained are shown in Table 5 as a function of the elements comprising the beam. The maximum membrane strains, ε_{max}, which exist throughout the beam at time = 1.3 msec after intercept are obtained from the NOVA-2L run. As shown in Figure 14, each element is assumed to recover from its maximum strain along a strain recovery line parallel to the elastic stress-strain segment of the curve. The residual strain is the value of the strain remaining at zero stress level, or the intercept of the recovery line with the σ=0 line. Additional columns in Table 6 give the derived quantities, where the maximum stress is

$$\sigma_{max} = \sigma_y + (\varepsilon_{max} - \varepsilon_Y)\, E_p$$

or

$$\sigma_{max} = 48{,}000 + (\varepsilon_{max} - 0.00457)\ 220{,}000 \text{ psi}$$

and the recoverable elastic strain is

$$\varepsilon_E = \frac{\sigma_{max}}{E_{elas}} = \sigma_{max} \left(\frac{\varepsilon_y}{\sigma_y}\right) = \sigma_{max} \left(\frac{0.00457}{48{,}000}\right)$$

The residual strain is

$$\varepsilon_R = \varepsilon_{max} - \varepsilon_E$$

and the elongation is

$$\Delta\ell = \ell\ \epsilon_R$$

The total elongation of the beam is twice the half-span elongation shown in the table

$$\Delta L_{TOT} = 2 \sum_i \Delta\ell_i = 2\ (0.026880) = 0.05376 \text{ in.}$$

With this residual elongation after encounter with the first blast, the deformed shape is assumed to be that of a catenary suspended at station x=0 and x=L under its own weight, such that

$$Z(x) = Z(x=\tfrac{L}{2})\quad [4\ \tfrac{x}{L}\ \ (\tfrac{L-x}{L})]$$

where

$$Z(x=\tfrac{L}{2}) = \tfrac{1}{4}\ \ \sqrt{6L\Delta L} = \tfrac{1}{4}\sqrt{6\ (8.5)\ 0.05376} = 0.414 \text{ in.}$$

Hence,

$$Z(x) = 0.414\ [4\ \tfrac{x}{8.5}\ (\tfrac{8.5-x}{8.5})] = 0.02292\ [x(8.5-x)]$$

The calculated values of vertical displacement Z are shown in the last column in Table 5.

Figure 15 shows the results of the first blast intercept graphically. Figure 15(a) presents the shape of the beam half-span (vertical displacements exaggerated) at time t = 1.3 msec, corresponding to the maximum membrane strains obtained (solid line), and the assumed shape after strain recovery. The latter is used as the initial shape for subsequent overpressure exposure in the sequential blast investigation. Figure 15(b) presents the displacement time history at the center of the beam, with a tick mark identifying the maximum membrane strain occurrence.

The permanently-deformed beam with the assumed shape of a catenary was then subjected to a second overpressure identical with the first blast overpressure. This would represent the limiting case, since for

simultaneous bursts the second arrival would imply a lesser range and smaller overpressure. The results of the second blast overpressure are shown in Figure 16. Figure 16(a) shows the assumed initial shape as a dashed curve, and the distorted shape at time = 1.79 msec after second blast arrival, corresponding to the generation of maximum membrane strains in all of the beam. The maximum values of incremental strains in all elements of the beam were under 0.0042 in/in, which is less than the yield strain of 0.00457 in/in. Thus, no new inelastic strains are imposed by the second blast of equal magnitude, and the post-blast beam returns to its initial catenary shape. Figure 16(b) shows the displacement time history at the center of the deformed beam, with a tick mark identifying the maximum membrane strain occurrence.

SECTION VI
THERMAL RADIATION ENVIRONMENT

6.1 Introduction

The enhanced nuclear thermal environment is discussed both in this section and in Section VII, where the combination of overpressure and thermal heating is considered. The thermal radiation environment used in this study is consistent with the nuclear scenario outlined earlier. In particular, the following assumptions are made:

1) Simultaneous 1 megaton bursts are detonated at sea level in one of two hexagonal close-packed patterns - either a seven burst hexagonal pattern (Figure 4), or a nineteen burst pattern shown in Figure 3.

2) The distance between burst centers was determined by the overpressure criterion that any aircraft within the close-pack region would be subjected to at least a two psi incident overpressure, which corresponds to a range of approximately 30,000 feet.

3) Escaping aircraft are assumed to be uniformly distributed throughout the region with random headings, so that only a small triangular planar section (Figure 5) need be studied. Individual flight paths are assumed to remain constant (no maneuver) for the duration of the thermal response, with horizontal velocity of 525 feet per second.

4) A very clear, dry atmosphere is assumed, with visibility equal to 100 miles.

In general, the analysis of thermal enhancement was intended to be conservative. It was for this reason that the "close-packed" burst pattern was selected, for example. Because thermal energy is radiated at the speed of light, a simultaneous detonation scenario was adopted. Here the seven burst configuration is probably the most likely laydown pattern, while the nineteen burst pattern comes into consideration for

interior portions of the country when warning times, and hence, escape times, would be longer.

Since side-on aircraft exposure is considered the most critical for a co-altitude burst, only side-on exposures (either left or right) were studied. This is consistent with the objective of the thermal study, which is to determine the enhancement due to the multiburst scenario compared with a worst-case single burst. This single burst can be any of the seven (or 19) multiburst positions, depending on the flight path. For the most part the central burst contributes the most thermal radiation for side-on exposure, although not always; an aircraft flying directly toward or away from the center being a prime example.

6.2 Methods of Analysis

Investigation of enhanced thermal effects due to the multiburst scenario relied primarily on the use of the computer code TRAP (Reference 6). TRAP is used ordinarily to calculate the thermal and stress response of structures to the thermal radiation from a single nuclear burst. For present purposes, however, it suffices to determine only the applicable thermal radiation environment; that is, the thermal fluence normally incident to the side of the aircraft.

In order to accommodate multiple exposures, the TRAP code was modified specifically to treat multiple simultaneous ground bursts of identical yield. As a practical matter the incident thermal flux was monitored for only ten seconds following detonation. However, approximately 90% of the energy associated with a 1MT burst has been emitted by that time.

As was the case in the gust analysis, nine aircraft positions were selected in a limited 30° triangular sector, with flight path headings every 30°. Only unique orientations were considered since there is considerable duplication due to symmetry. The aircraft velocity was assumed to be 525 ft/sec.

Since only side-on exposures were considered, both left and right side thermal fluences (for the 10 second interval) were calculated, and the larger value used for comparison. For single burst cases the most severe single burst among the seven (or 19) positions was used.

6.3 Results of Analysis

Table 6 summarizes the results for single burst, seven burst, and 19 burst environments. In each instance, the side of the aircraft receiving the larger thermal fluence is indicated L for left, R for right, as well as the total incident thermal fluence received in ten seconds.

Fluence levels for 19 burst cases are consistently larger than for seven bursts, which, in turn, are consistently larger than the single burst results. This has to be so due to the symmetrical arrangement of burst centers and because thermal radiation is strictly additive, i.e., there is no cancellation effect. Additional rings of bursts contribute less and less the further away they are due to atmospheric attenuation and the inverse square law.

As indicated earlier, the fluence levels in Table 6 represent only approximately 90% of the total thermal pulse. This was determined by extending one response run for 100 seconds, as compared with the ten second runs used in the study. Figure 17 indicates the shape of the incident thermal pulse for the nearest aircraft location. This correction factor was then applied to the tabulated results, and the envelopes in Figure 18 were generated.

These peanut-shaped envelopes represent the level of incident thermal fluence for both the worst single burst case and the 19 burst exposure. For the nine burst-time aircraft positions indicated by the large dots, an envelope represents the side-on exposure for any aircraft heading. Envelopes for headings not shown in Figure 18 can be determined from symmetry considerations.

This survey of aircraft exposure to incident thermal radiation indicates that while there is overall enhancement due to multiple bursts, there is no significant change in the envelope patterns. Consequently, without addressing the question of actual vulnerability levels, it is concluded that the enhancement derived from the additional bursts is characterized by slightly higher levels and more uniformly shaped envelopes of thermal fluence.

SECTION VII
COUPLED THERMAL/OVERPRESSURE ENVIRONMENT

7.1 Introduction

Previous sections have dealt with the individual nuclear effects of gust, overpressure, and thermal radiation. In some instances the combined effect of thermal radiation, which preheats and prestresses the aircraft structure, followed by a blast wave can produce critical response in skin panels.

The thermal pulse propagates at the speed of light, so the aircraft begins receiving the thermal radiation almost immediately following the first burst. At some later time the blast wave from that burst arrives; by that time the skin temperature will be elevated to some extent. Also, for multiple burst cases, thermal input from the other bursts may be contributing to the temperature rise, depending on the timing of these bursts. Subsequent blast waves are not considered important as long as the nearest burst (and therefore the strongest shock) is assumed to detonate first.

A survey of the "worst-case" environments, similar to that performed for the pure thermal response, was made for both a single central burst, and for the seven burst close-packed laydown pattern. As a worst-case assumption, the central burst is assumed to occur first, with the remaining bursts all simultaneously detonating at a later time. That time delay is determined by considering the shock arrival time at each of the nine aircraft locations studied, and the time it takes to build up the maximum temperature rise following a 1MT burst.

Obviously, the delay assumed between bursts must be consistent with a realistic laydown plan. Preliminary studies by RDA (Reference 3) indicate that the maximum delay time used here (15.5 seconds) is possible, especially for bases located in the interior United States.

7.2 Method of Analysis

Program TRAP was further modified to study the enhancement of combined thermal-overpressure effects. Since the multiple bursts were no longer assumed to arrive simultaneously, allowance was made for a delay between the central burst and the remaining bursts. Then, since the time history of the temperature rise in the skin is important, the effect of absorptivity and the effect of convective cooling were also included in the analysis.

As a typical example, an absorptivity of 0.5 was assumed for an aluminum skin panel 0.04 in. thick, located 10 feet behind the leading edge of the vertical tail. The vertical tail location is susceptible to side-on exposure, consistent with the pure thermal analysis.

From various computer runs it was determined that approximately five seconds were required from time of burst to reach a peak panel temperature. Consequently, the six surrounding bursts in the seven burst laydown pattern were assumed to detonate roughly five seconds before the arrival of the blast wave from burst number one, the central burst. This maximizes the temperature difference between the single and multiple burst cases at blast wave arrival.

The side of the vertical tail directly exposed to the central burst was selected for study. Comparisons were then made between the temperature rises at time of shock arrival for the multiple burst environment versus the single burst case. Since this study is exploratory in nature, the analysis did not continue on to determine and compare structural responses. Rather, the temperature comparison is considered to be indicative of the possibility of enhanced thermal/overpressure coupling.

7.3 Results of Analysis

The results of the survey sixty-six aircraft flight paths are tabulated in Table 7. The last two columns indicate the temperature in the skin panel at time of shock arrival for both single and multiple burst environments.

Enhancement is evident for all orientations, particularly for those cases where little single-burst heating takes place. For flight paths involving single burst temperature rises of 250° R or more, the increases were all less than 32%. Another way of looking at this is to realize that the maximum multiple burst temperature rise of 464° R compares with 388° R maximum for all single burst cases - a difference of only 76° R.

Figure 19 illustrates the sequence of events. Bursts 2-7 are assumed to detonate seven seconds after the center burst, the shock from which arrives an additional five seconds later. Even though the aircraft location selected is the closest of all considered, the shock still arrives too late (12 seconds) to impinge on the skin before significant cooling has begun.

SECTION VIII
CONCLUSIONS

The analysis of gust, overpressure, and thermal radiation effects on aircraft in a base escape mode was limited in scope to an investigation of the enhancement or attenuation of the effects due to multiple burst exposure in comparison with a single "critical burst" exposure. The multiple bursts were assumed to be laid down in a hexagonal close-packed configuration and were detonated simultaneously except for considering the worst case blast-thermal coupling enhancement.

In the side gust-effects analysis, enhancement due to multiple bursts was observed in very limited cases and was small in magnitude. However, definite attenuation was observed to occur for aircraft flight paths where side gusts arrived simultaneously from opposite directions due to symmetrically-placed simultaneous bursts of equal yield, thus cancelling each other. This attenuation would be greatly affected if the aircraft flight path were offset such that the shock fronts did not arrive simultaneously.

The effect of multiple bursts is thus generally quite small for gust response, and the area in which the effect is large (attenuation) is very limited in extent. Hence, multiple burst effects are of little consequence with respect to aircraft gust vulnerability.

In the overpressure effects analysis, the structural panel response differences between single and multiple burst cases were less than 10% and are considered insignificant. The response of stringers located near surface boundaries can be significantly enhanced by the multiple burst environment. An analysis of cumulative damage due to sequential overpressure exposure was carried out on idealized beam-element strips representing panels. Where the first blast encounter caused permanent deformation, a subsequent identical blast exposure imposed no additional permanent strain, indicating no additional damage due to multiple blast exposure.

Multiple burst effects for overpressure damage thus appear to be unimportant for skin panels, the effect being both small and localized. The picture is less clear with respect to stringers. Large enhancement can occur, but again the regions involved are small and so the overall impact on system vulnerability is also probably small. Sequential overpressure exposure could result in increased damage to stringers and other structures, even though it apparently does not for skin panels. The investigation herein of skin panels treated membranes only, and structural elements which do not respond as membranes may well behave very differently with respect to sequential exposure. Examination of this problem in the present exploratory study was impossible because of the lack of codes which can reasonably handle this problem. In this respect, it will be recalled that a special treatment had to be concocted to deal with the membrane problem. In the absence of any analysis, only an educated guess i possible. The authors expect that sequential exposure will result in significantly enhanced damage to stringers and the like, but that the importance with respect to overall vulnerability will be small because the vulnerability will be affected in only a small portion of the total area or volume involved. It is suggested, therefore, that further investigation of this point is appropriate, but as a low priority item.

In the thermal radiation exposure investigation, overall enhancement due to multiple exposure was observed, but the shape of the envelopes of thermal fluence was not changed significantly. The results of the combined thermal/overpressure exposure analysis indicated that the worst-case situations, where the blast wave from the closest burst arrived at the time when the thermal exposure from other bursts caused peak temperatures, resulted in enhancements of less than 32% in peak temperature in comparison to a single burst for cases in which the single burst temperature was greater than $250^{\circ}R$.

It is apparent that multiple burst effects are more important for thermal damage than for gust or overpressure alone. Analysis of thermal response to multiple bursts is a relatively simple problem, however. It

is recommended, therefore, that TRAP be modified to permit multiple bursts to be treated. The modifications made for the purpose of the present analysis do not suffice, since they lack generality.

REFERENCES

1. Hobbs, N. P., Thompson, J. H., Ruetenik, J. R., MULTIFLECT Code for Computing Interaction of Two Bursts, Kaman AviDyne TR-118, DNA 3949F, October 1975.

2. Thompson, J. H., Dalton, T. A., Walsh, J. P., Ruetenik, J. R., Comparison of Interceptor Multiburst Environments, Kaman AviDyne TR-115, January 1975.

3. Hurley, J. W., Bomber Base Escape: Multiburst Environment, R&D Associates, Marina Del Rey, California. Private communication, December 1976.

4. Needham, C. E., and Wittwer, L. A., Editors, Low Altitude Multiple Burst (LAMB) Model, Air Force Weapons Laboratory, AFWL-DYT-TN-75-2.

5. Lee, W. N., A User's Manual for NOVA-2L, Kaman AviDyne TM-109, May 1977.

6. Hobbs, N. P., TRAP - A Digital Computer Program for Calculating The Response of Aircraft to the Radiation From a Nuclear Explosion, Air Force Weapons Laboratory, AFWL-TR-71-61, Vol. 1, October 1972.

TABLE 1

SIDE GUST ENVIRONMENT AND RESPONSE FOR SEVEN SIMULTANEOUS BURSTS

CASE I.D. (LOCATION AND ORIENTATION)	PEAK GUST (FT/SEC)	@ TIME (SEC)	1 HZ RESPONSE		5 HZ RESPONSE	
			MAXIMUM DISPL. (10^{-3} FT)	@ TIME (SEC)	MAXIMUM DISPL. (10^{-3} FT)	@ TIME (SEC)
1.090	36.15	46.49	3.84	46.49	0.16	46.59
1.120	34.03	17.02	3.44	29.36	0.15	28.99
1.150	59.49	17.02	6.41	31.23	0.27	30.85
1.180	0.00	34.29	0.00	34.78	0.00	34.39
2.090	39.80	44.30	4.24	44.78	0.18	44.40
2.120	110.13	17.80	6.43	25.18	0.29	24.81
2.150	93.24	25.76	8.55	26.23	0.38	25.85
2.180	81.01	27.73	8.29	28.21	0.35	27.83
2.210	65.38	30.74	6.40	31.22	0.27	30.84
2.240	35.15	17.80	3.78	33.99	0.17	17.93
2.270	0.00	47.75	0.00	18.24	0.00	17.90
3.210	0.00	20.47	0.00	20.95	0.00	20.56
3.240	38.66	20.45	3.76	48.71	0.16	48.34
3.270	0.00	50.40	0.00	50.44	0.00	50.44
4.000	0.00	42.20	0.00	42.87	0.00	42.48
4.030	69.79	14.49	8.17	14.97	0.35	14.59
4.060	120.71	14.49	13.95	14.97	0.60	14.59
4.090	139.68	14.48	15.87	14.95	0.69	14.58
4.120	120.90	21.24	13.50	14.95	0.59	14.57
4.150	77.59	30.89	7.83	31.37	0.34	14.57
4.180	0.00	43.40	0.00	43.88	0.00	43.50
5.000	82.22	28.29	8.35	28.77	0.35	28.39
5.030	95.09	25.74	8.54	26.19	0.38	25.84
5.060	94.38	15.17	11.73	20.09	0.46	15.27
5.090	128.79	15.17	14.71	15.65	0.63	15.27
5.120	128.62	15.17	14.43	15.64	0.63	15.26
5.150	94.51	15.16	10.45	15.63	0.46	15.25
5.180	69.73	29.32	7.56	29.81	0.32	29.42
5.210	62.74	22.81	6.69	23.28	0.28	22.91
5.240	125.52	21.09	11.37	21.55	0.51	21.19
5.270	128.62	15.17	14.59	20.24	0.63	15.26
5.300	128.79	15.17	14.71	15.65	0.63	15.27
5.330	94.38	15.17	10.95	15.65	0.46	15.27

TABLE 1 (CONT'D)

SIDE GUST ENVIRONMENT AND RESPONSE FOR SEVEN SIMULTANEOUS BURSTS

CASE I.D. (LOCATION AND ORIENTATION)	PEAK GUST (FT/SEC)	@ TIME (SEC)	1 HZ RESPONSE		5 HZ RESPONSE	
			MAXIMUM DISPL. (10^{-3}FT)	@ TIME (SEC)	MAXIMUM DISPL. (10^{-3}FT)	@ TIME (SEC)
6.210	0.00	23.84	0.00	24.32	0.00	23.94
6.240	112.16	22.37	10.87	22.83	0.47	22.47
6.270	101.25	21.39	11.04	17.97	0.48	17.59
6.300	115.80	17.50	12.98	17.97	0.56	17.60
6.330	100.41	17.50	11.45	17.98	0.49	17.60
6.000	60.68	20.74	9.36	22.49	0.34	22.06
6.030	0.00	21.15	0.00	21.64	0.00	21.25
7.000	0.00	-	0.00	-	0.00	-
7.030	83.85	11.98	9.97	12.46	0.42	12.08
7.060	145.04	11.98	17.02	12.45	0.73	12.08
7.090	167.87	11.97	19.36	12.44	0.84	12.06
7.120	145.20	11.97	16.44	12.44	0.73	12.06
7.150	106.77	31.37	10.32	31.82	0.42	12.06
7.180	0.00	41.66	0.00	41.96	0.00	41.76
8.000	77.10	29.20	7.98	29.67	0.33	29.30
8.030	68.15	29.16	7.07	29.62	0.29	22.61
8.060	113.13	12.56	13.00	13.03	0.57	12.65
8.090	154.54	12.56	17.75	13.03	0.77	12.65
8.120	154.54	12.56	17.75	13.03	0.77	12.65
8.150	113.13	12.56	12.99	13.03	0.57	12.65
8.180	76.92	29.22	8.01	29.70	0.33	29.32
8.210	67.41	29.26	6.96	29.72	0.29	22.68
8.240	113.13	12.56	12.99	13.03	0.57	12.65
8.270	154.54	12.56	17.75	13.03	0.77	12.65
8.300	154.54	12.56	17.75	13.03	0.77	12.65
8.330	113.13	12.56	13.00	13.03	0.57	12.65
9.210	0.00	40.37	0.00	40.86	0.00	40.47
9.240	86.68	25.12	9.31	25.60	0.38	25.22
9.270	120.13	14.56	13.41	15.03	0.59	14.65
9.300	138.89	14.56	15.77	15.03	0.68	14.66
9.330	120.03	14.57	13.86	15.05	0.59	14.67
9.000	90.97	23.47	10.43	23.97	0.42	23.57
9.030	0.00	21.88	0.00	22.36	0.00	21.98

TABLE 2

SIDE GUST ENVIRONMENT AND RESPONSE FOR
SELECTED SINGLE "CRITICAL BURST"

CASE I.D. (LOCATION AND ORIENTATION)	PEAK GUST (FT/SEC)	@ TIME (SEC)	1 HZ RESPONSE		5 HZ RESPONSE	
			MAXIMUM DISPL. (10^{-3} FT)	@ TIME (SEC)	MAXIMUM DISPL. (10^{-3} FT)	@ TIME (SEC)
1.090	119.22	17.02	13.39	17.49	0.58	17.12
1.120	103.12	17.02	11.39	17.49	0.50	17.11
1.150	60.50	30.75	6.53	31.23	0.28	30.85
1.180	56.69	34.29	6.20	34.77	0.26	34.39
2.090	109.89	17.81	12.41	18.29	0.53	17.91
2.120	110.13	17.80	12.23	18.27	0.53	17.90
2.150	71.27	25.76	7.73	26.23	0.33	25.86
2.180	71.73	27.73	7.89	28.21	0.33	27.83
2.210	80.48	17.81	9.23	18.29	0.39	17.91
2.240	109.85	17.81	12.41	18.29	0.53	17.91
2.270	110.13	17.80	12.23	18.27	0.53	17.91
3.210	85.74	20.47	9.68	20.95	0.41	20.57
3.240	99.12	20.46	11.01	20.94	0.47	20.56
3.270	85.71	20.46	9.37	20.93	0.41	20.55
4.000	57.57	34.01	6.29	34.49	0.26	34.11
4.030	69.79	14.49	8.17	14.97	0.35	14.59
4.060	120.71	14.49	13.95	14.97	0.60	14.59
4.090	139.68	14.48	15.87	14.95	0.69	14.58
4.120	120.89	14.48	13.50	14.95	0.59	14.57
4.150	69.76	14.48	7.69	14.95	0.34	14.57
4.180	53.44	35.35	5.86	35.83	0.25	35.45
5.000	70.53	28.29	7.74	28.77	0.33	28.39
5.030	69.72	25.74	7.55	26.21	0.32	25.84
5.060	94.38	15.17	10.95	15.65	0.46	15.27
5.090	128.79	15.17	10.47	15.65	0.63	15.27
5.120	128.62	15.17	14.43	15.64	0.63	15.26
5.150	94.51	15.16	10.45	15.63	0.46	15.25
5.180	65.91	29.32	7.26	29.80	0.31	29.42
5.210	53.67	35.61	5.79	36.09	0.25	35.71
5.240	94.51	15.16	10.45	15.63	0.46	15.25
5.270	128.62	15.17	14.43	15.64	0.63	15.26
5.300	128.79	15.17	14.71	15.65	0.63	15.27
5.330	94.38	15.17	10.95	15.65	0.46	15.27

TABLE 2 (CONT'D)

SIDE GUST ENVIRONMENT AND RESPONSE FOR
SELECTED SINGLE "CRITICAL BURST"

CASE I.D. (LOCATION AND ORIENTATION)	PEAK GUST (FT/SEC)	@ TIME (SEC)	1 HZ RESPONSE		5 HZ RESPONSE	
			MAXIMUM DISPL. (10^{-3} FT)	@ TIME (SEC)	MAXIMUM DISPL. (10^{-3} FT)	@ TIME (SEC)
6.210	64.89	23.84	7.30	24.32	0.31	23.94
6.240	89.10	22.37	9.91	22.85	0.42	22.47
6.270	100.16	17.50	11.04	17.97	0.48	17.59
6.300	115.80	17.50	12.98	17.97	0.56	17.60
6.330	100.41	17.50	11.45	17.98	0.49	17.60
6.000	92.11	21.96	10.19	22.44	0.44	22.06
6.030	80.74	21.15	8.80	21.62	0.38	21.25
7.000	58.28	33.79	6.36	34.27	0.27	33.89
7.030	83.85	11.98	9.97	12.46	0.42	12.08
7.060	145.04	11.98	17.02	12.45	0.73	12.08
7.090	167.87	11.97	19.36	12.44	0.84	12.06
7.120	145.20	11.97	16.44	12.44	0.73	12.06
7.150	83.75	11.97	9.36	12.43	0.42	12.06
7.180	49.19	36.90	5.40	37.38	0.23	37.00
8.000	67.83	29.20	7.42	29.68	0.31	29.30
8.030	57.31	22.51	6.33	22.99	0.27	22.61
8.060	113.13	12.56	13.00	13.03	0.57	12.65
8.090	154.54	12.56	17.75	13.03	0.77	12.65
8.120	154.54	12.56	17.75	13.03	0.77	12.65
8.150	113.13	12.56	12.99	13.03	0.57	12.65
8.180	67.80	29.22	7.41	29.70	0.31	29.32
8.210	56.99	22.58	6.30	23.06	0.27	22.68
8.240	113.13	12.56	12.99	13.03	0.57	12.65
8.270	154.54	12.56	17.75	13.03	0.77	12.65
8.300	154.54	12.56	17.75	13.03	0.77	12.65
8.330	113.13	12.56	13.00	13.03	0.57	12.65
9.210	47.17	28.29	5.28	28.77	0.22	28.39
9.240	75.97	25.12	8.44	25.60	0.36	25.22
9.270	120.13	14.56	13.41	15.03	0.59	14.65
9.300	138.89	14.56	15.77	15.03	0.68	14.66
9.330	120.03	14.57	13.86	15.05	0.59	14.67
9.000	86.04	23.47	9.48	23.95	0.40	23.57
9.030	75.99	21.86	8.26	22.35	0.36	21.98

TABLE 3

COMPARISON OF SIDE GUST ENVIRONMENT AND RESPONSE FOR SEVEN SIMULTANEOUS BURSTS VS. SELECTED SINGLE "CRITICAL BURST"

CASE I.D. (LOCATION AND ORIENTATION)	GUST RATIO	DISPLACEMENT RATIO	
		1 HZ RESPONSE	5 HZ RESPONSE
1.090	0.30	0.29	0.28
1.120	0.33	0.30	0.30
1.150	0.98	0.98	0.98
1.158	0.00	0.00	0.00
2.090	0.36	0.34	0.34
2.120	1.00	0.53	0.54
2.150	1.31	1.11	1.15
2.180	1.13	1.05	1.06
2.210	0.81	0.69	0.69
2.240	0.32	0.31	0.32
2.270	0.00	0.00	0.00
3.210	0.00	0.00	0.00
3.240	0.39	0.34	0.34
3.270	0.00	0.00	0.00
4.000	0.00	0.00	0.00
4.030	1.00	1.00	1.00
4.060	1.00	1.00	1.00
4.090	1.00	1.00	1.00
4.120	1.00	1.00	1.00
4.150	1.11	1.02	1.00
4.180	0.00	0.00	0.00
5.000	1.17	1.08	1.06
5.040	1.37	1.13	1.19
5.060	1.00	1.07	1.00
5.090	1.00	1.00	1.00
5.120	1.00	1.00	1.00
5.150	1.00	1.00	1.00
5.180	1.06	1.04	1.03
5.210	1.17	1.16	1.14
5.240	1.33	1.09	1.10
5.270	1.00	1.01	1.00
5.300	1.00	1.00	1.00
5.330	1.00	1.00	1.00

CASE I.D. (LOCATION AND ORIENTATION)	GUST RATIO	DISPLACEMENT RATIO	
		1 HZ RESPONSE	5 HZ RESPONSE
6.210	0.00	0.00	0.00
6.240	1.26	1.10	1.12
6.270	1.01	1.00	1.00
6.300	1.00	1.00	1.00
6.330	1.00	1.00	1.00
6.000	0.66	0.92	0.79
6.030	0.00	0.00	0.00
7.000	0.00	0.00	0.00
7.030	1.00	1.00	1.00
7.060	1.00	1.00	1.00
7.090	1.00	1.00	1.00
7.120	1.00	1.00	1.00
7.150	1.28	1.10	1.00
7.180	0.00	0.00	0.00
8.000	1.14	1.08	1.07
8.030	1.19	1.12	1.07
8.060	1.00	1.00	1.00
8.090	1.00	1.00	1.00
8.120	1.00	1.00	1.00
8.150	1.00	1.00	1.00
8.180	1.14	1.08	1.07
8.210	1.18	1.11	1.07
8.240	1.00	1.00	1.00
8.270	1.00	1.00	1.00
8.300	1.00	1.00	1.00
8.330	1.00	1.00	1.00
9.210	0.00	0.00	0.00
9.240	1.14	1.10	1.06
9.270	1.00	1.00	1.00
9.300	1.00	1.00	1.00
9.330	1.00	1.00	1.00
9.000	1.06	1.10	1.05
9.030	0.00	0.00	0.00

TABLE 4

SINGLE AND MULTI-BURST RESPONSE COMPARISONS USING A LOADING GENERATED BY LAMB FOR A PANEL AND STRINGER FROM A REPRESENTATIVE AIRCRAFT

REFLECTED PRESSURE (PSI)	CHARACTERISTIC DECAY TIME (SEC)	DISTANCE FROM LEADING EDGE (FT)	MAX. DEFL. (IN)	%DIFF.	MAX STRAIN (IN/IN)	%DIFF.
FLAT PANEL						
5.1	3.75	-	.19		.00544	
5.1	.0055	2	.183	3.8	.00507	7.3
5.1	.0164	6	.188	1.1	.00532	2.3
5.1	.0327	12	.189	.5	.00538	1.1
STRINGER						
5.1	3.75	-	1.08		-.0641	
5.1	.0055	2	.85	27.0	-.0244	163.0
5.1	.0164	6	.98	10.2	-.0525	22.1
5.1	.0327	12	1.02	5.9	-.0595	7.7

TABLE 5

INELASTIC RESPONSE DUE TO BLAST OVERPRESSURE

MASS #	STATION X (IN)	ℓ (IN)	ε_{MAX} (IN/IN)	σ_{MAX} (PSI)	ε_E	ε_R	$\Delta\ell$ (μ IN)	DISTORTED Z (IN)
		0.25	0.0120356	49,642.432	0.0047264	0.0073092	1,827	
1	-3.75	0.50	0.0120356	49,642.432	0.0047264	0.0073092	3,655	-0.091672
2	-3.25	0.50	0.0116949	49,567.478	0.0047192	0.0069757	3,488	-0.171885
3	-2.75	0.50	0.0112593	49,471.646	0.0047101	0.0065492	3,275	-0.240639
4	-2.25	0.50	0.0108887	49,390.114	0.0047024	0.0061863	3,093	-0.297934
5	-1.75	0.50	0.0106285	49,332.870	0.0046969	0.0059316	2,966	-0.343770
6	-1.25	0.50	0.0104502	49,293.644	0.0046932	0.0057570	2,879	-0.378147
7	-0.75	0.50	0.0103870	49,279.740	0.0046918	0.0056952	2,848	-0.401065
8	-0.25	0.50	0.0103899	49,280.378	0.0046919	0.0056980	2,849	-0.412524
						HALF-SPAN ΔL =26,880 (μIN)		-0.413957

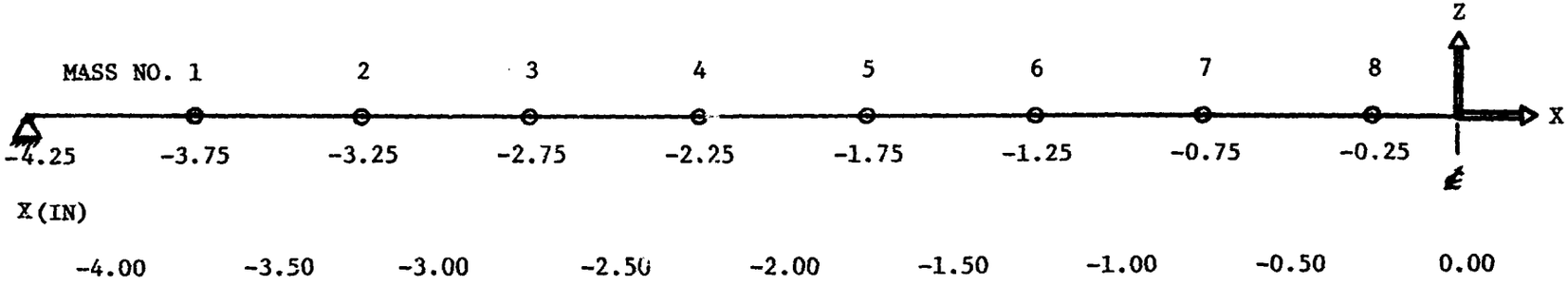

TABLE 6

INCIDENT THERMAL FLUENCE FOR MULTIPLE BURST COMPARISONS

AIRCRAFT LOCATION X(FT)	AIRCRAFT LOCATION Y(FT)	AIRCRAFT HEADING* (DEG)	SINGLE BURST NO.*	SINGLE BURST SIDE*	SINGLE BURST Q*	7 BURSTS SIDE*	7 BURSTS Q*	19 BURSTS SIDE*	19 BURSTS Q*
20,000	0	0	6	L	6.96	L	10.06	L	13.93
		30	1	L	20.95	L	30.44	L	33.69
		60	1	L	38.56	L	46.71	L	49.59
		90	1	L	48.91	L	55.03	L	57.77
		120	1	L	47.34	L	55.12	L	57.97
		150	1	L	30.18	L	39.22	L	42.41
		180	5	L	6.78	L	10.53	L	14.31
20,000	5359	0	1	R	9.92	R	20.06	R	23.65
		30	7	R	11.32	L	21.74	L	25.18
		60	1	[illegible]	8.21	L	37.48	L	40.54
		90	1	[illegible]	4..62	L	47.83	L	50.60
		120	1	L	46.10	L	53.34	L	56.06
		150	1	L	37.54	L	45.13	L	48.14
		180	1	L	14.78	L	24.27	L	27.78
		210	1	R	14.78	R	25.83	R	29.21
		240	1	R	37.54	R	46.18	R	49.18
		270	1	R	46.10	R	52.25	R	55.01
		300	1	R	41.62	R	49.04	R	51.77
		330	1	R	28.21	R	36.07	R	39.13
20,000	11,547	0	1	R	15.36	R	26.57	R	29.89
		30	6	L	11.86	L	16.58	L	20.29
		210	7	L	9.99	L	15.31	L	18.97
		240	1	R	21.20	R	31.31	R	34.55
		270	1	R	33.73	R	40.08	R	42.89
		300	1	R	35.31	R	42.25	R	44.86
		330	1	R	28.11	R	34.59	R	37.45
23,000	0	0	6	L	7.07	L	9.74	L	13.72
		30	1	L	15.49	L	25.00	L	28.26
		60	1	L	28.36	L	36.63	L	39.44
		90	1	L	35.64	L	41.31	L	43.97
		120	1	L	34.06	L	41.89	L	44.65
		150	1	L	21.41	L	30.46	L	33.66
		180	5	L	6.98	L	10.01	L	13.89

TABLE 6 (CONT'D)

INCIDENT THERMAL FLUENCE FOR MULTIPLE BURST COMPARISONS

AIRCRAFT LOCATION X(FT)	AIRCRAFT LOCATION Y(FT)	HEADING* (DEG)	SINGLE BURST NO.*	SINGLE BURST SIDE*	SINGLE BURST Q*	7 BURSTS SIDE*	7 BURSTS Q*	19 BURSTS SIDE*	19 BURSTS Q*
23,000	6163	0	6	L	10.21	R	18.90	R	22.57
		30	7	R	14.86	R	19.81	R	24.04
		60	1	L	20.78	L	30.67	L	33.70
		90	1	L	30.42	L	36.19	L	38.89
		120	1	L	33.33	L	40.42	L	43.04
		150	1	L	26.78	L	34.09	L	37.08
		180	1	L	10.43	L	20.90	L	24.46
		210	7	L	11.92	R	22.04	R	25.47
		240	1	R	14.98	R	35.86	R	38.83
		270	1	R	33.33	R	39.04	R	41.72
		300	1	R	30.42	R	37.71	R	40.35
		330	1	R	20.78	R	28.33	R	31.39
23,000	13,279	0	6	L	16.71	R	24.44	R	27.78
		30	6	L	14.71	L	18.80	L	22.61
		210	7	L	12.50	L	17.05	L	20.79
		240	7	L	16.24	R	26.51	R	29.77
		270	1	R	24.11	R	30.02	R	32.79
		300	1	R	25.54	R	32.22	R	34.73
		330	1	R	20.51	R	26.53	R	29.35
26,000	0	90	1	L	26.83	L	32.22	L	34.82
		120	1	L	25.38	L	33.25	L	35.96
		150	1	L	15.79	L	24.80	L	28.04
		180	5	L	7.08	L	9.71	L	13.71
26,000	6967	90	1	L	22.97	L	28.49	L	31.13
		120	1	L	24.94	L	31.85	L	34.38
		150	1	L	19.83	L	26.83	L	29.83
		180	6	R	10.77	L	19.77	L	23.41
		210	7	L	15.78	L	20.78	L	25.10
		240	7	L	22.97	R	29.44	R	32.37
		270	1	R	24.94	R	30.39	R	33.00
26,000	15,011	210	7	L	15.45	L	19.40	L	23.24
		240	7	L	19.10	R	24.50	R	27.79
		270	1	R	17.88	R	23.65	R	26.38

TABLE 6 (CONT'D)

INCIDENT THERMAL FLUENCE FOR MULTIPLE BURST COMPARISONS

* - Definitions:

(1) Heading is defined with 0^{o} coinciding with positive X axis, and 90^{o} coinciding with the positive Y axis.

(2) Burst numbers are defined as follows:

NO.	X	Y
1	0	0
2	-52,000	0
3	-26,000	-45,000
4	-26,000	+45,000
5	+26,000	-45,000
6	+26,000	+45,000
7	+52,000	0

(3) Thermal fluence (Q) in cal/cm^2 represents total incident thermal radiation after 10 seconds.

(4) Side refers to the side of the aircraft exposed:

L - Left

R - Right

TABLE 7

TEMPERATURE RISE AT TIME OF BLAST ARRIVAL
FOR SINGLE BURST AND DELAYED SEVEN BURST CASE

AIRCRAFT LOCATION X(FT)	AIRCRAFT LOCATION Y(FT)	AIRCRAFT HEADING (DEG)	SIDE EXPOSED	SHOCK ARRIV. TIME, TA (SEC)	DELAY BETWEEN FIRST AND REMAINING BURSTS (SEC)	ΔT@ TA FOR SINGLE BURST (°R)	ΔT@ TA FOR 7 BURSTS (°R)
20,000	0	0	L	11.96	7.0	6	96
		30	L			149	253
		60	L			292	384
		90	L			388	453
		120	L			385	464
		150	L			244	332
		180	L			11	99
20,000	5359	0	R	12.55	7.5	65	180
		30	L			65	196
		60	L			200	308
		90	L			312	378
		120	L			359	433
		150	L			296	372
		180	L			113	202
		210	R			113	216
		240	R			296	380
		270	R			359	422
		300	R			312	393
		330	R			200	285
20,000	11,547	0	R	14.55	9.5	90	235
		30	L			3	195
		210	L			6	127
		240	R			148	237
		270	R			232	296
		300	R			234	307
		330	R			176	245
23,000	0	0	L	14.47	9.5	3	93
		30	L			91	196
		60	L			178	275
		90	L			236	295
		120	L			234	310
		150	L			149	234
		180	L			[illegible]	94

TABLE 7 (CONT'D)

TEMPERATURE RISE AT TIME OF BLAST ARRIVAL
FOR SINGLE BURST AND DELAYED SEVEN BURST CASE

AIRCRAFT LOCATION X(FT)	AIRCRAFT LOCATION Y(FT)	AIRCRAFT HEADING (DEG)	SIDE EXPOSED	SHOCK ARRIV. TIME, TA (SEC)	DELAY BETWEEN FIRST AND REMAINING BURSTS (SEC)	ΔT@ TA FOR SINGLE BURST (^{o}R)	ΔT@ TA FOR 7 BURSTS (^{o}R)
23,000	6163	0	R	15.16	10	40	193
		30	L			40	182
		60	L			121	245
		90	L			189	249
		120	L			217	288
		150	L			180	251
		180	L			70	161
		210	R			70	172
		240	R			180	262
		270	R			217	275
		300	R			189	270
		330	R			121	203
23,000	13,279	0	R	17.49	12.5	52	256
		30	L			2	237
		210	L			3	132
		240	R			86	178
		270	R			134	192
		300	R			135	205
		330	R			102	166
26,000	0	90	L	17.01	12.0	147	203
		120	L			146	219
		150	L			94	176
		180	L			3	92
26,000	6967	90	L	17.79	12.8	113	172
		120	L			130	198
		150	L			109	175
		180	L			43	138
		210	R			43	146
		240	R			109	190
		270	R			130	185
26,000	15,011	210	L	20.44	15.5	2	139
		240	R			52	147
		270	R			80	134

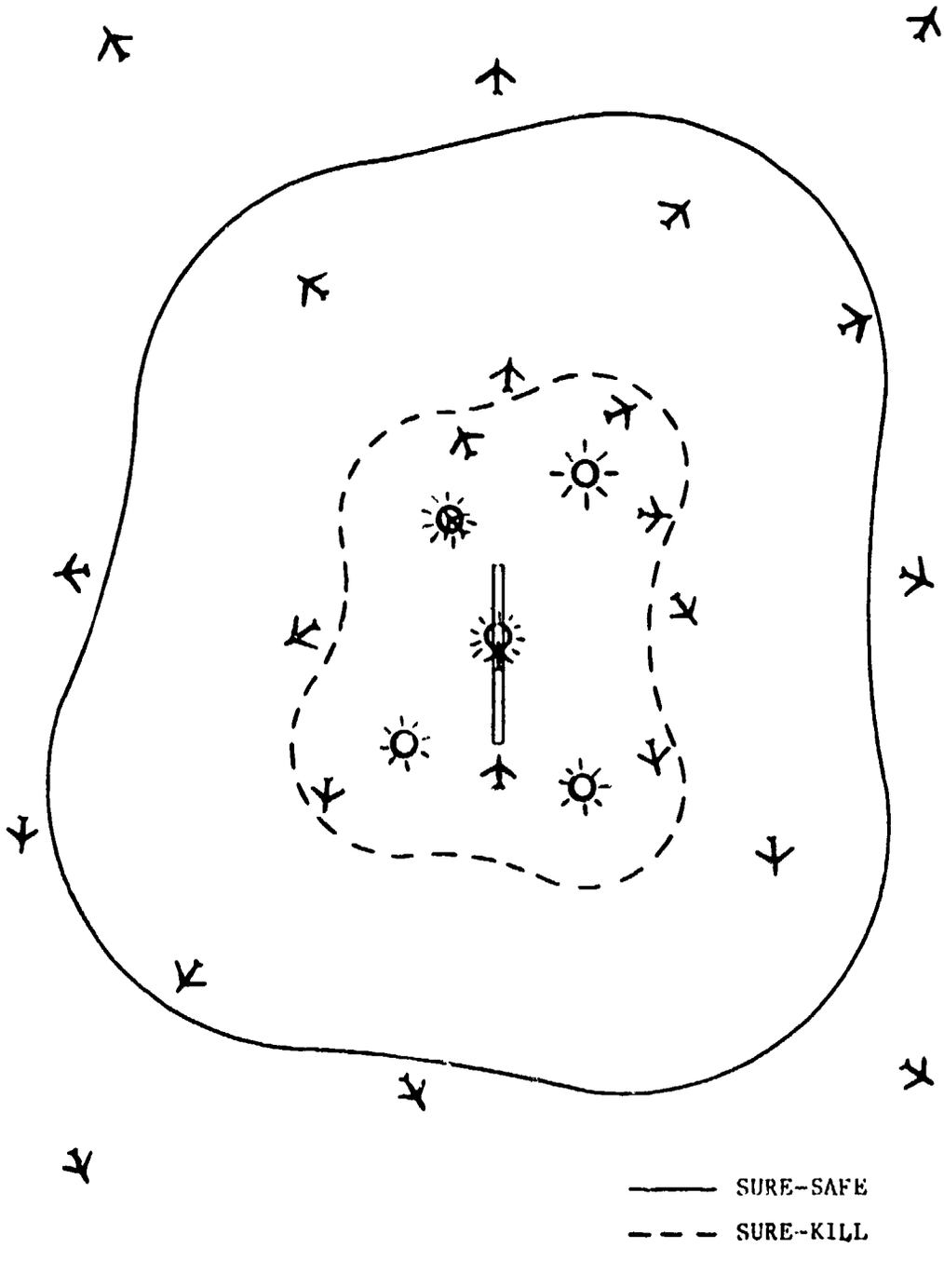

FIGURE 1. HYPOTHETICAL ILLUSTRATION OF AN AIRCRAFT BASE UNDER SLBM ATTACK

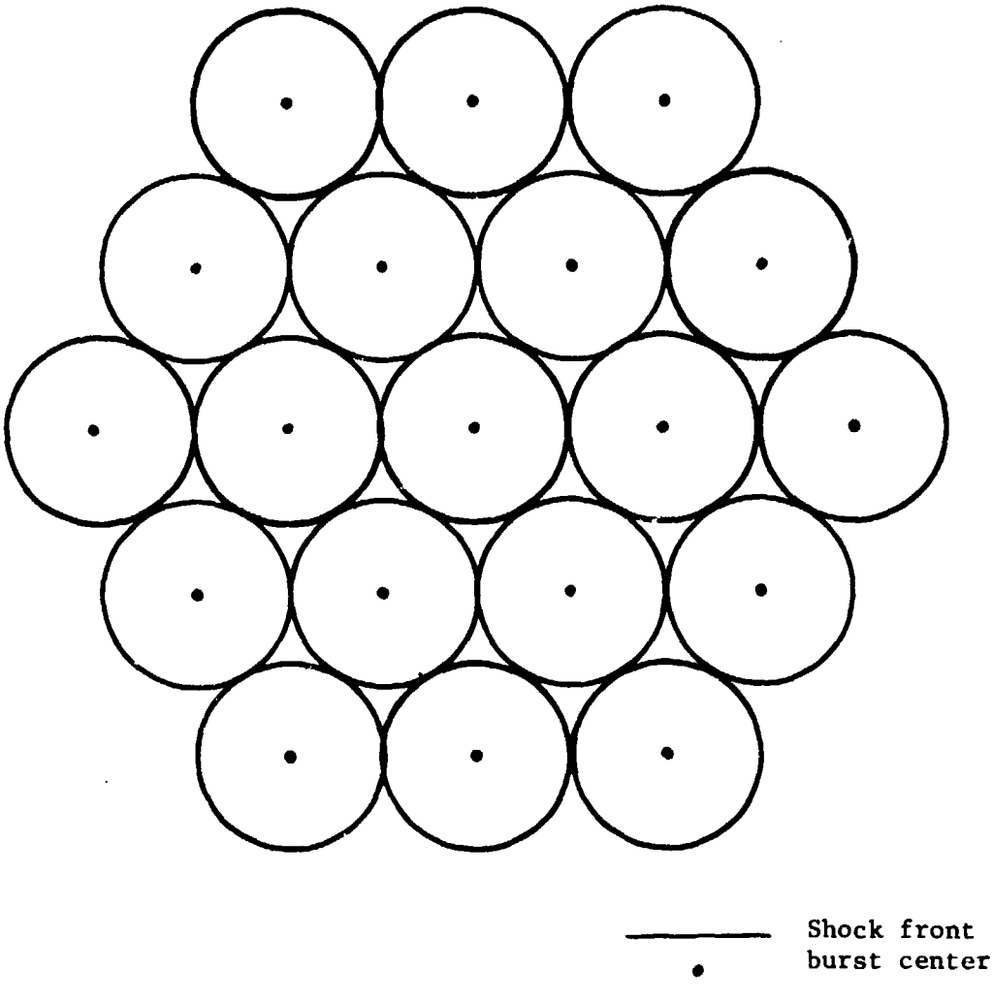

FIGURE 2. HEXAGONAL CLOSE-PACKED LAYDOWN PATTERN SHOWING SHOCK FRONTS JUST PRIOR TO OVERLAP

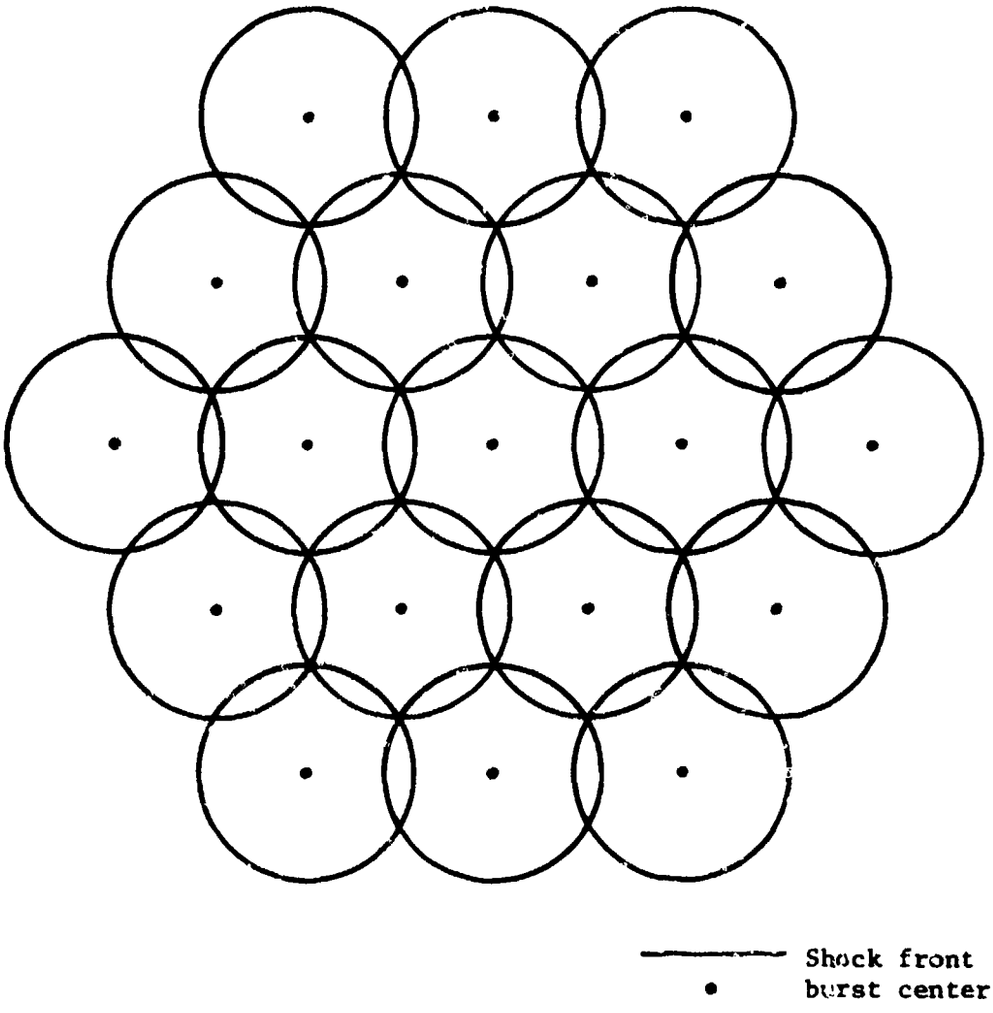

FIGURE 3. HEXAGONAL CLOSE-PACKED LAYDOWN PATTERN SHOWING OVERLAPPING SHOCK FRONTS

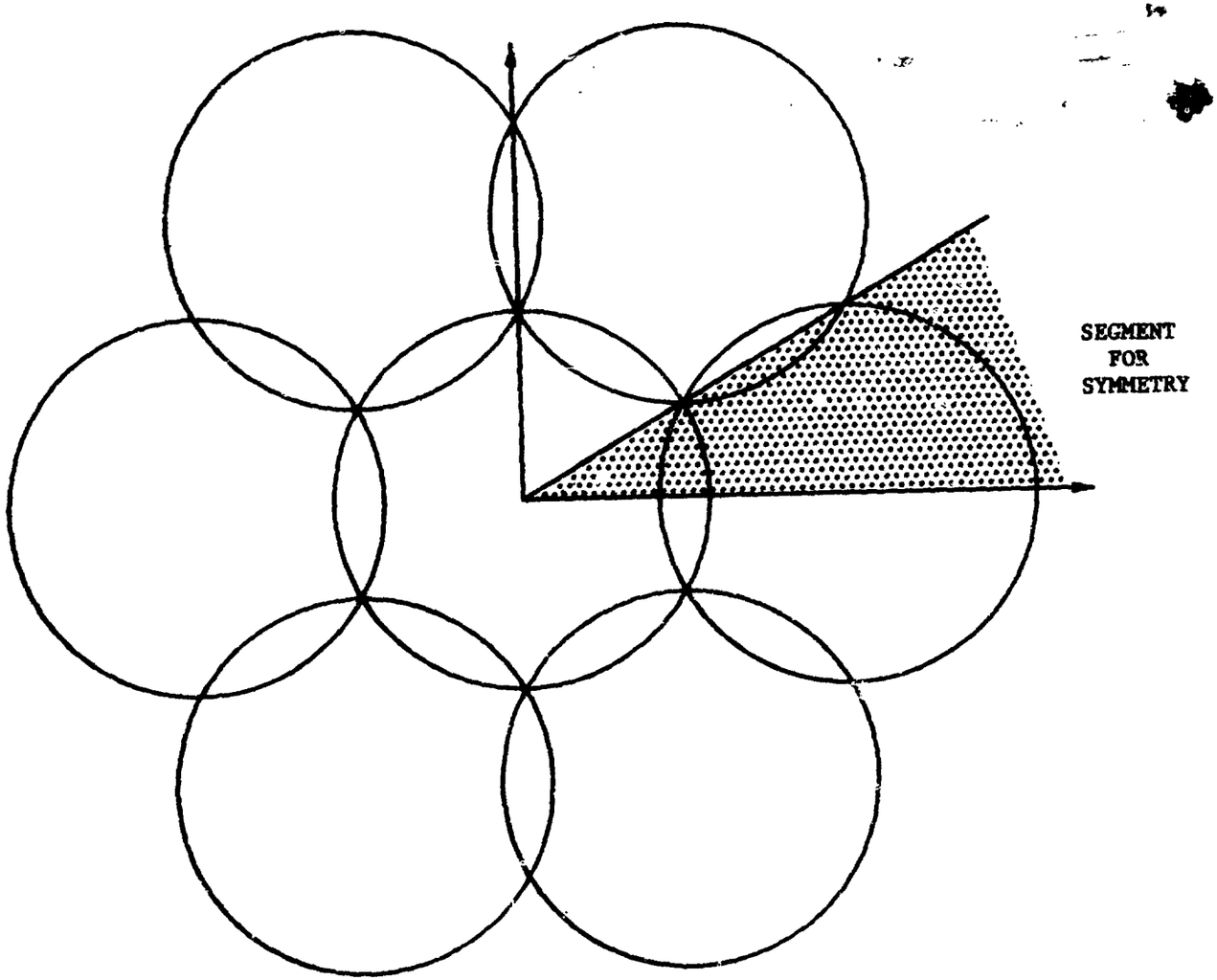

FIGURE 4. HEXAGONAL CLOSE-PACKED LAYDOWN FOR SEVEN SIMULTANEOUS BURSTS, SHOWING SEGMENT FOR SYMMETRY

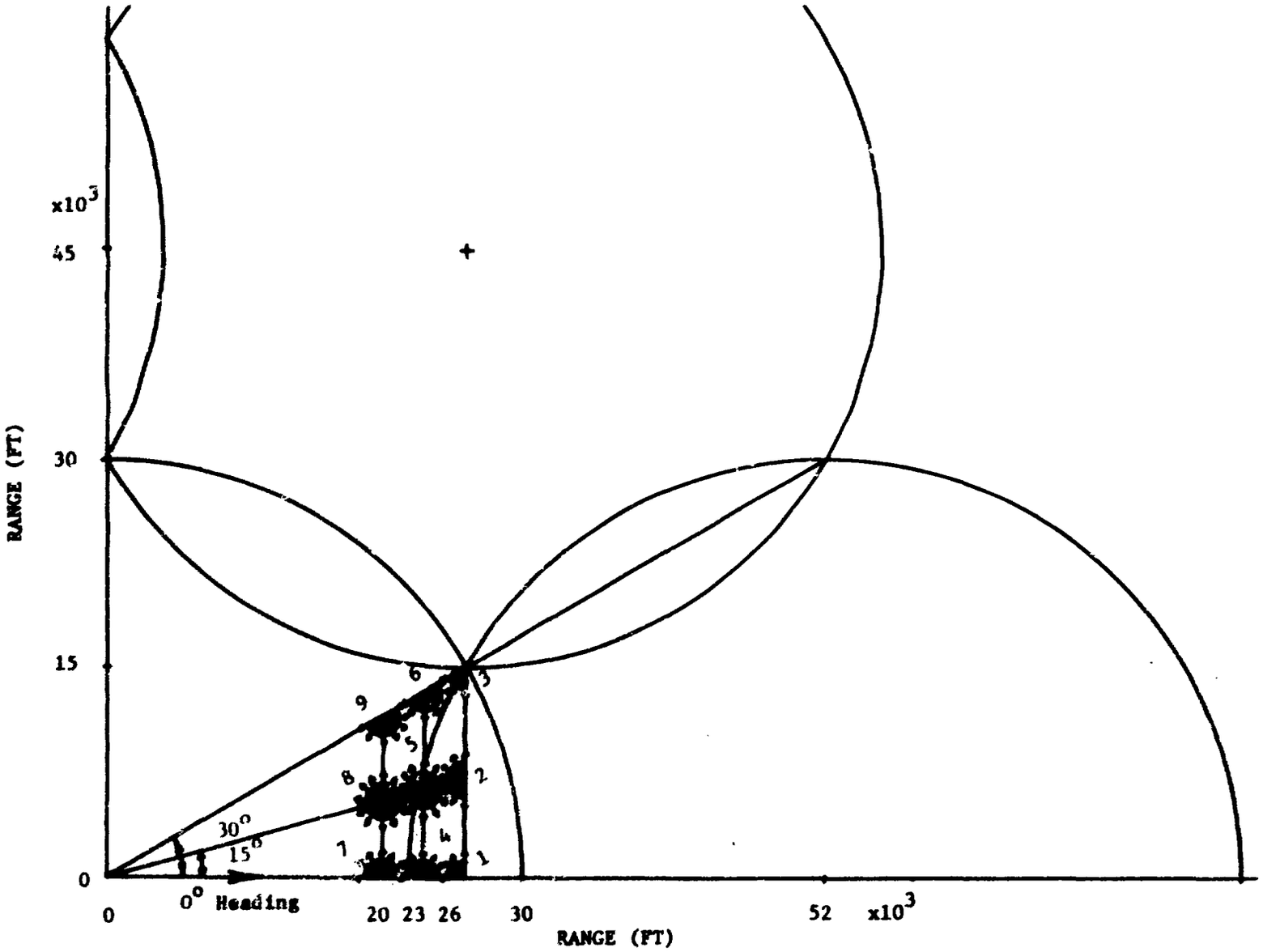

FIGURE 5. MULTIPLE BURST SEGMENT FOR SYMMETRY, SHOWING AIRCRAFT POSITION AND FLIGHT PATH ORIENTATION

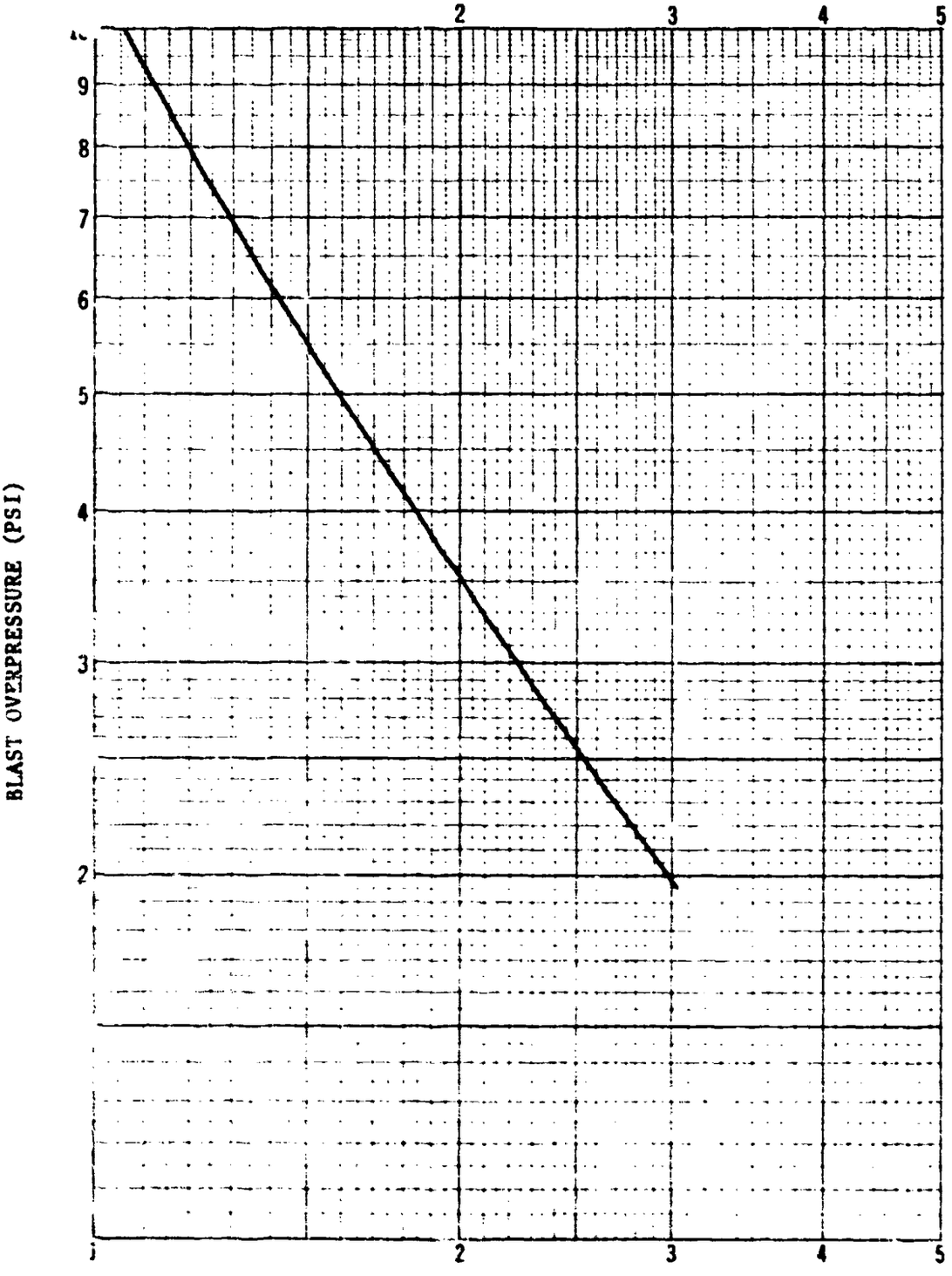

FIGURE 6. BLAST-GENERATED PEAK OVERPRESSURE VS. RANGE FROM BLAST CENTER FOR A LAMB 1 MT YIELD BURST WITH GROUND REFLECTION

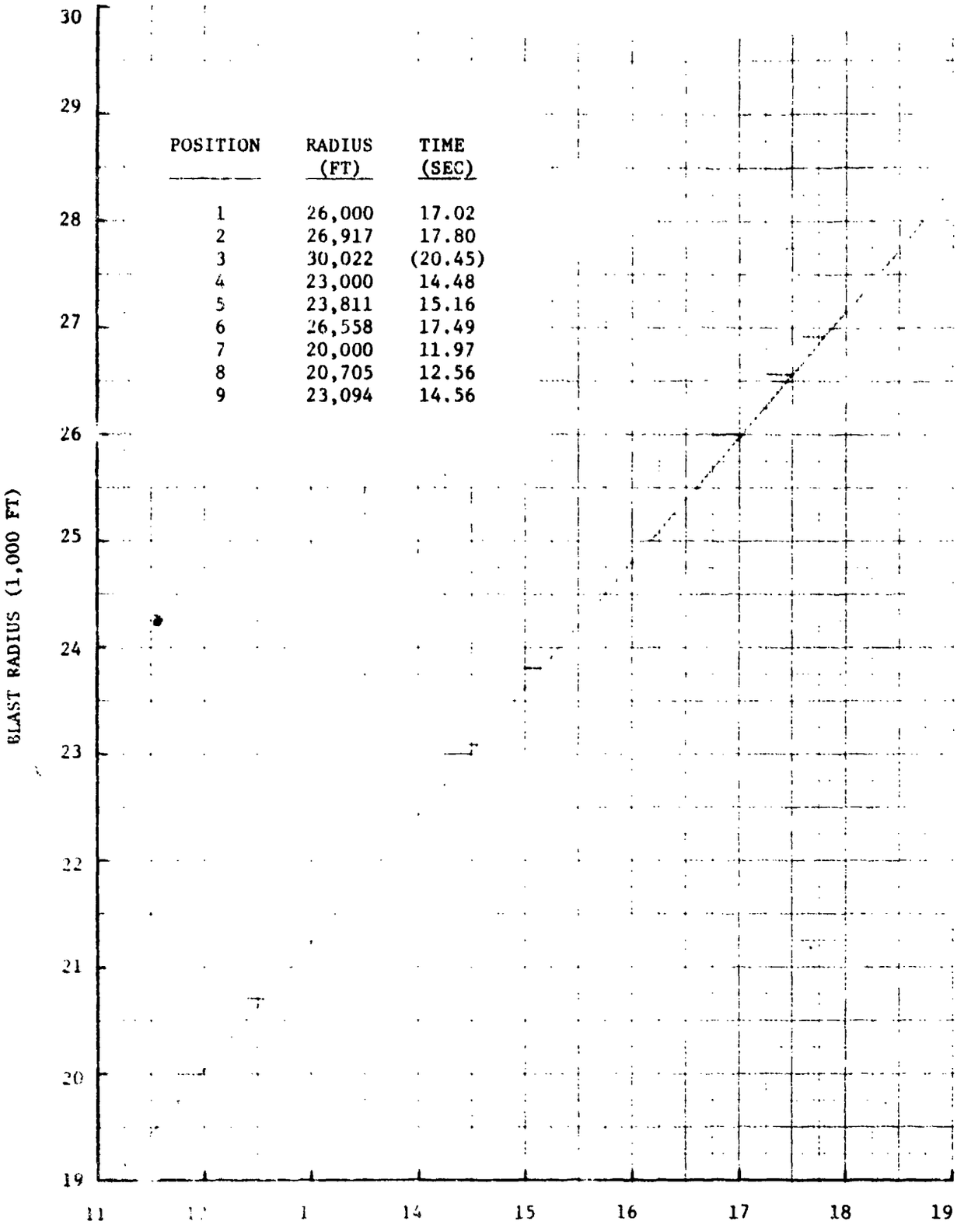

POSITION	RADIUS (FT)	TIME (SEC)
1	26,000	17.02
2	26,917	17.80
3	30,022	(20.45)
4	23,000	14.48
5	23,811	15.16
6	26,558	17.49
7	20,000	11.97
8	20,705	12.56
9	23,094	14.56

FIGURE 7. BLAST RADIUS VS. TIME AFTER BURST
FOR 1 MT YIELD BURST LAMB CALCULATION

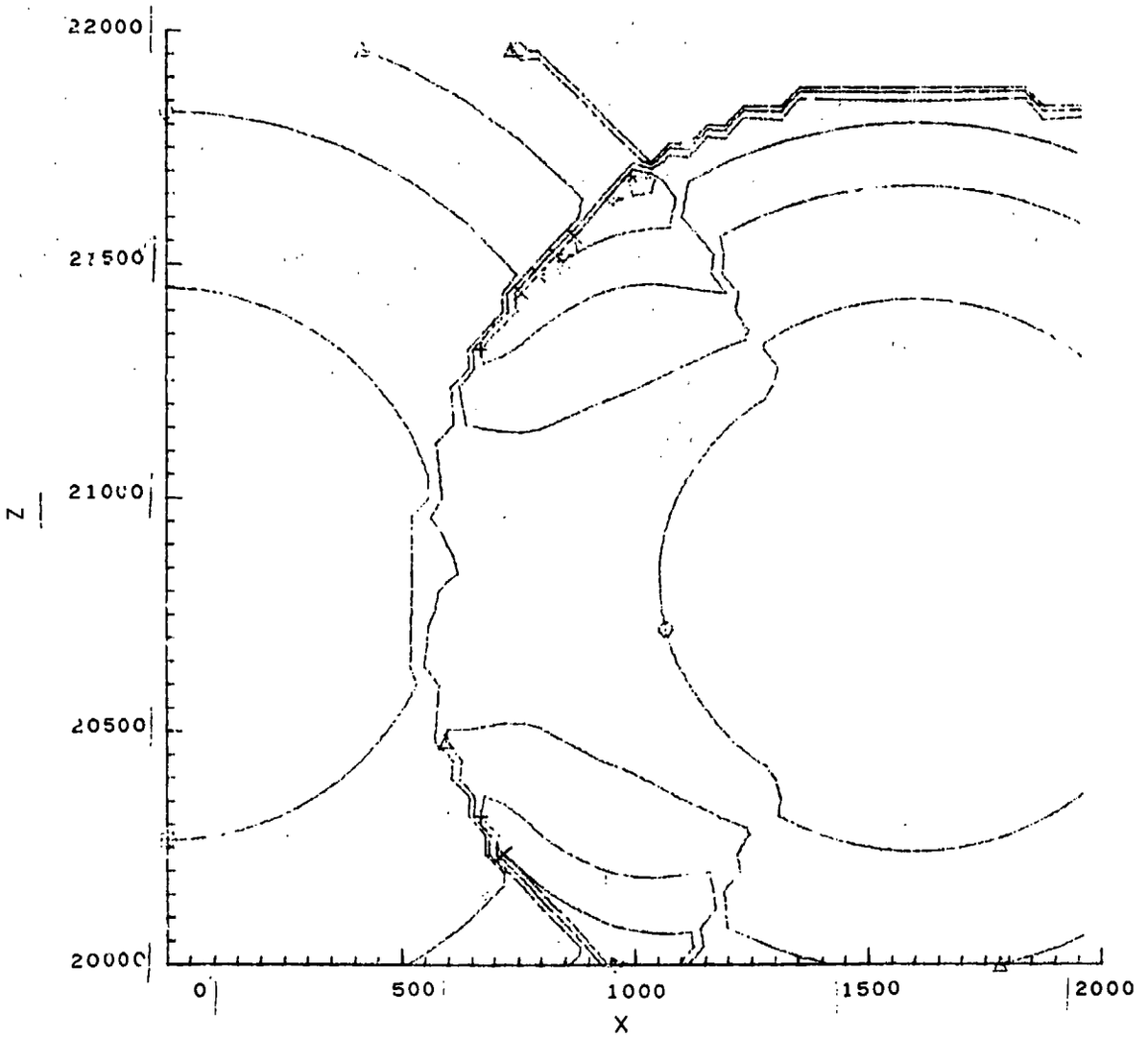

(a) Pressure Contours

FIGURE 8. PRESSURE AND DENSITY CONTOURS, AND MATERIAL VELOCITY VECTORS FOR TWO INTERACTING BLASTS

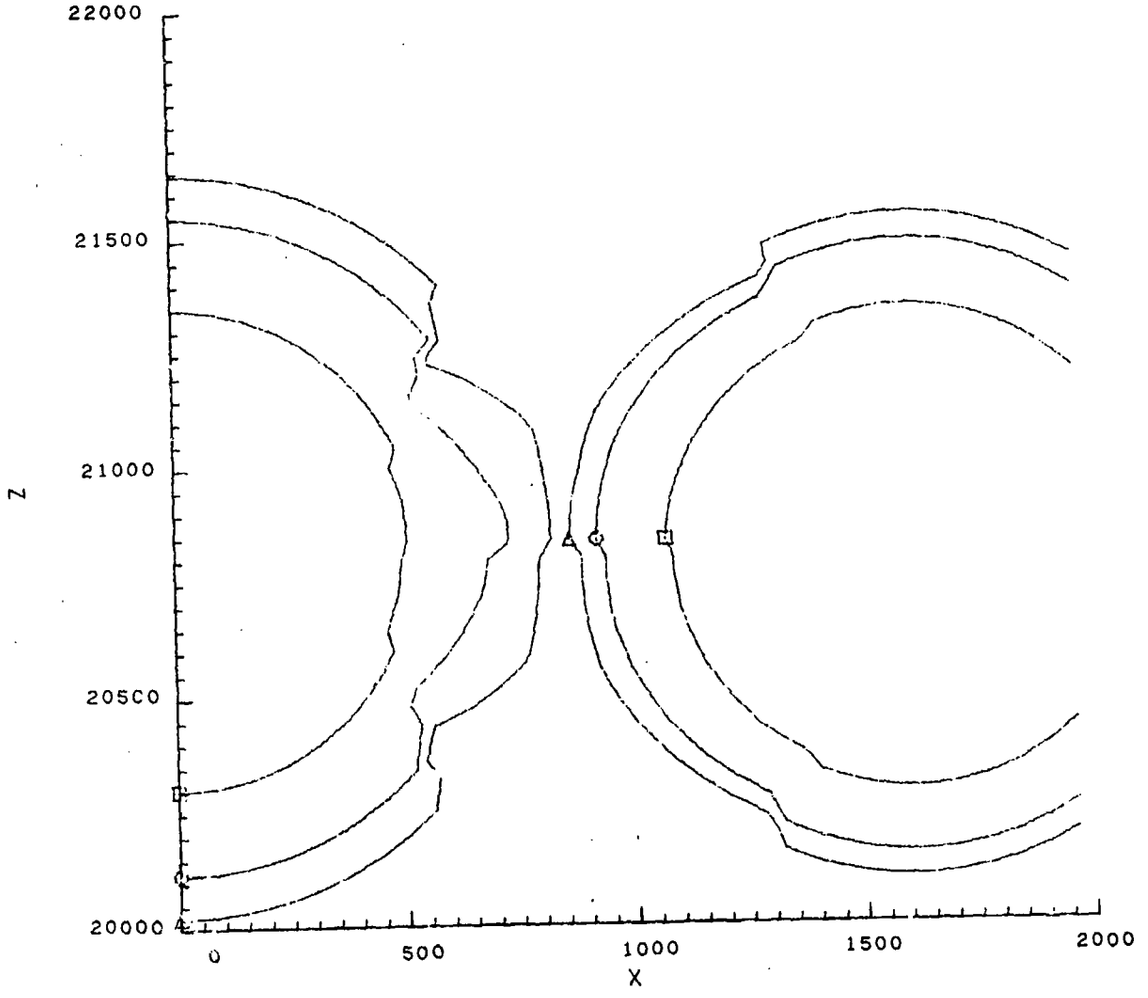

(b) Density Contours

FIGURE 8. CONTINUED

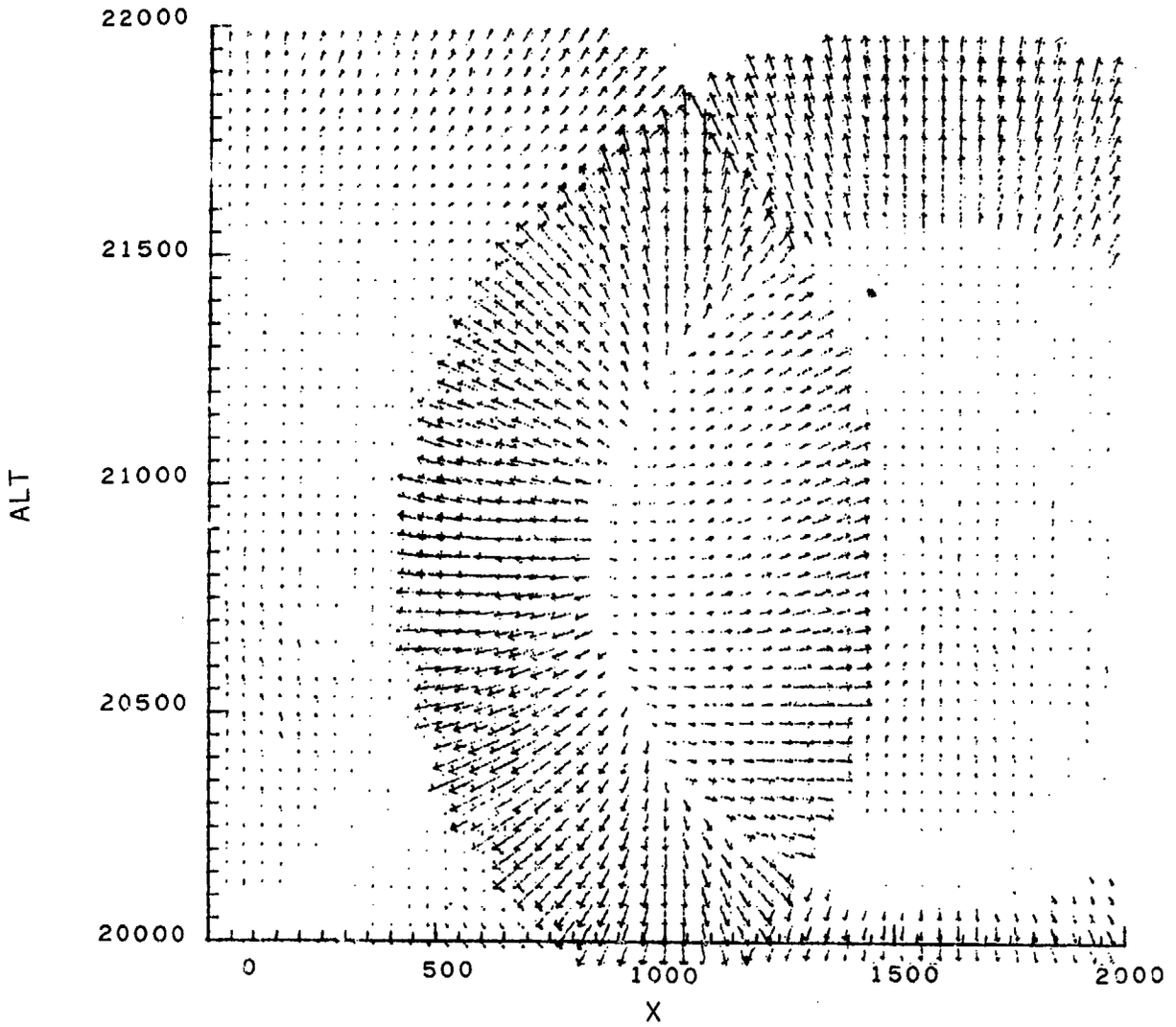

(c) Material Velocity Vectors

FIGURE 8. CONCLUDED

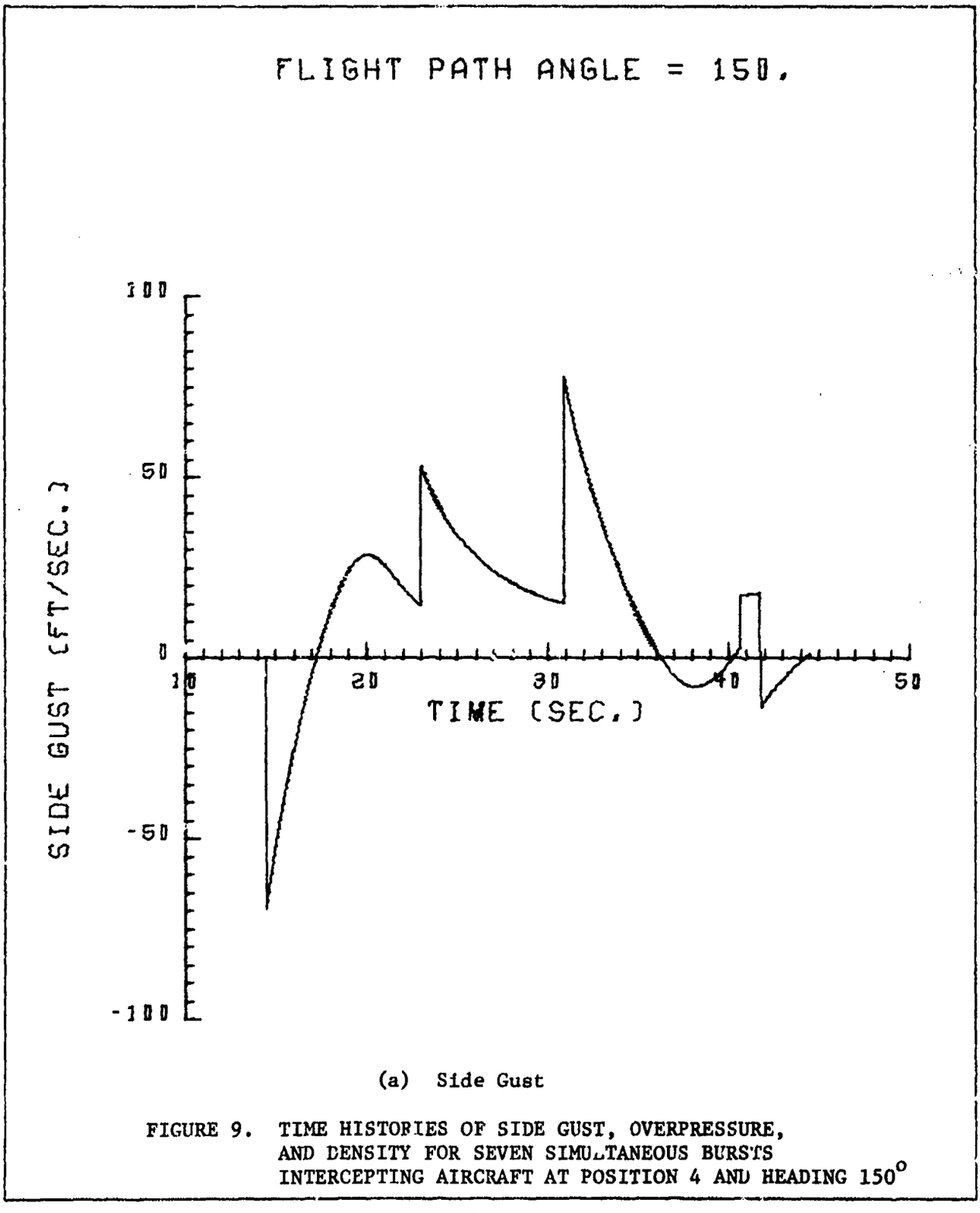

(a) Side Gust

FIGURE 9. TIME HISTORIES OF SIDE GUST, OVERPRESSURE, AND DENSITY FOR SEVEN SIMULTANEOUS BURSTS INTERCEPTING AIRCRAFT AT POSITION 4 AND HEADING 150°

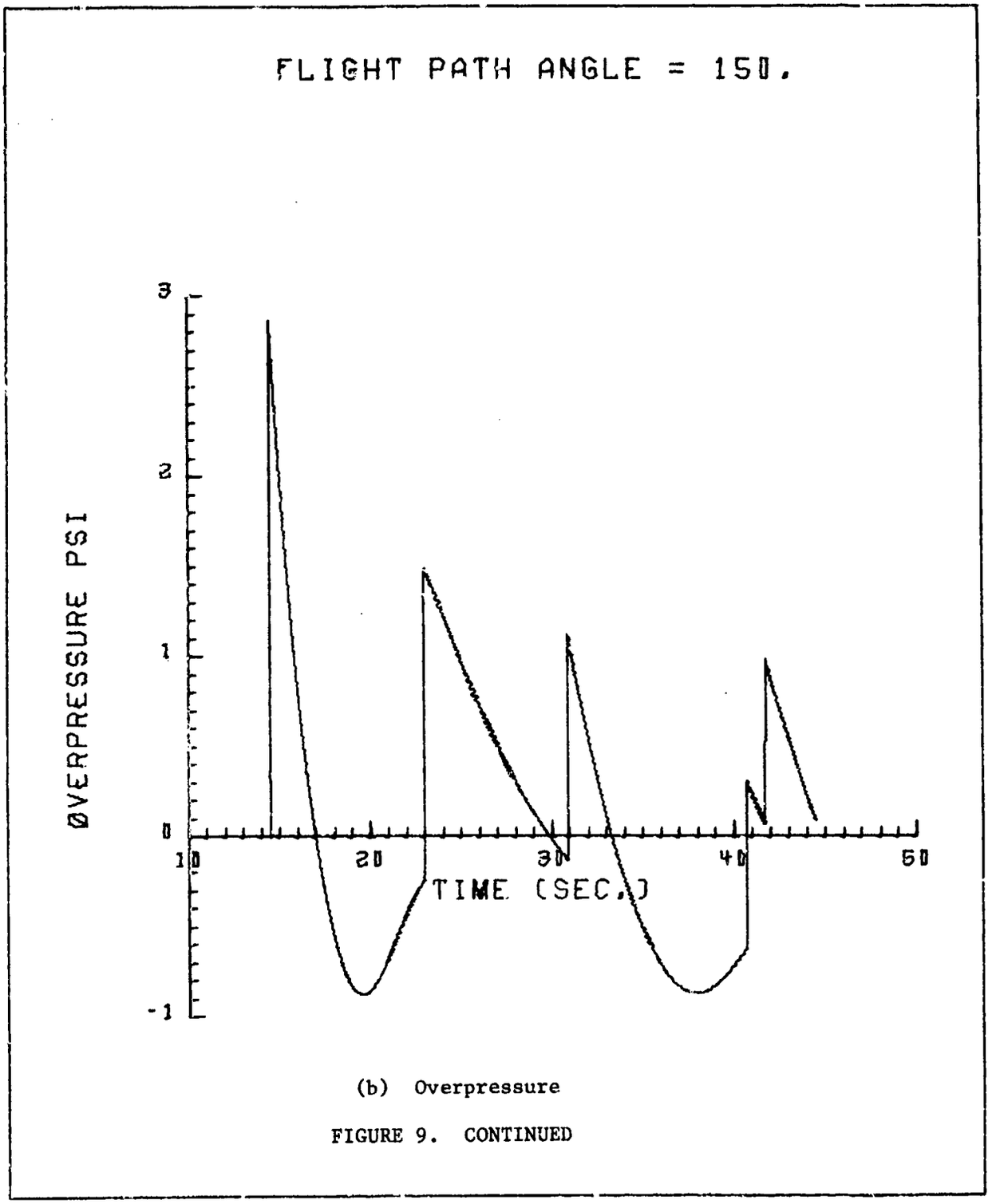

(b) Overpressure

FIGURE 9. CONTINUED

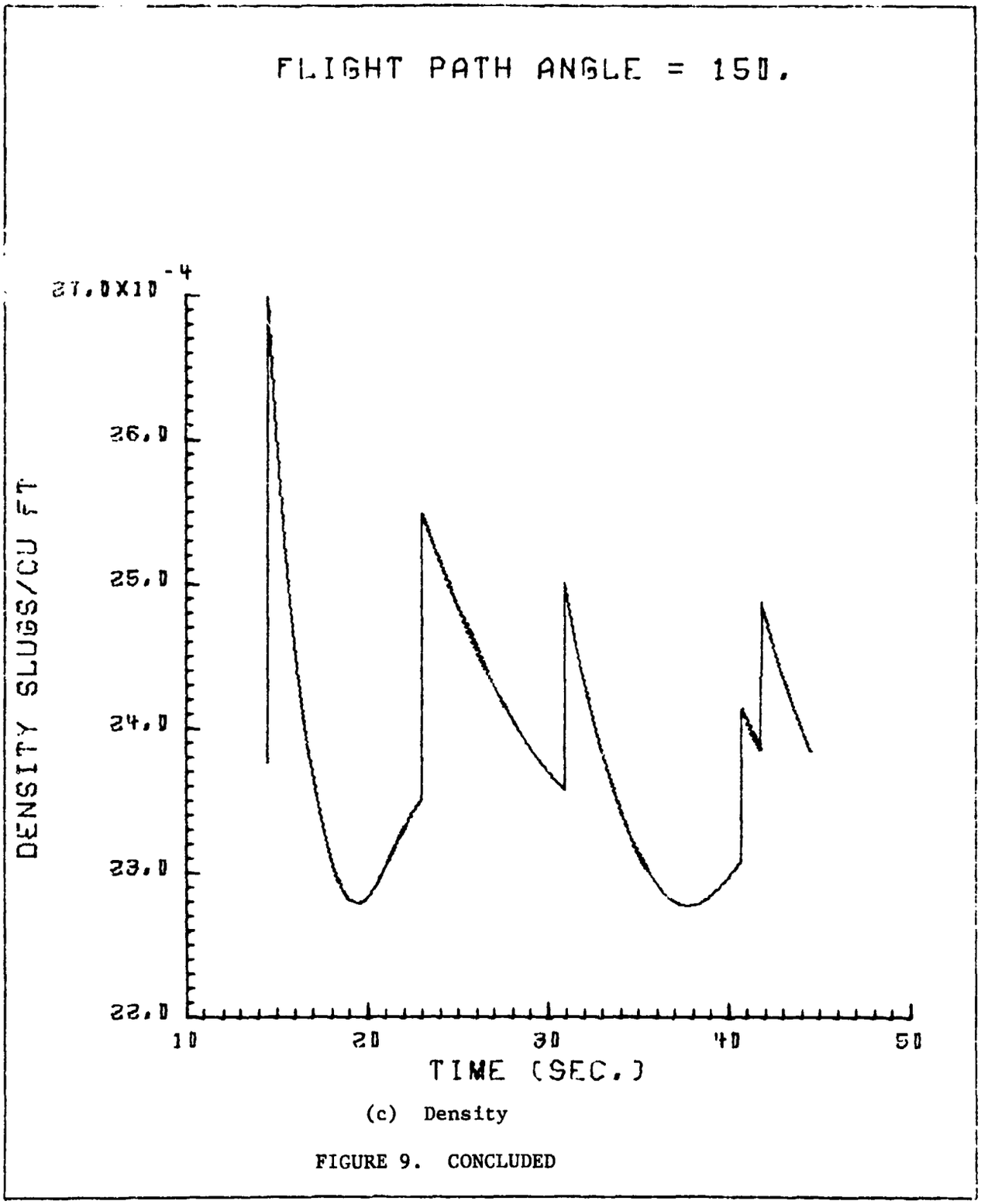

(c) Density

FIGURE 9. CONCLUDED

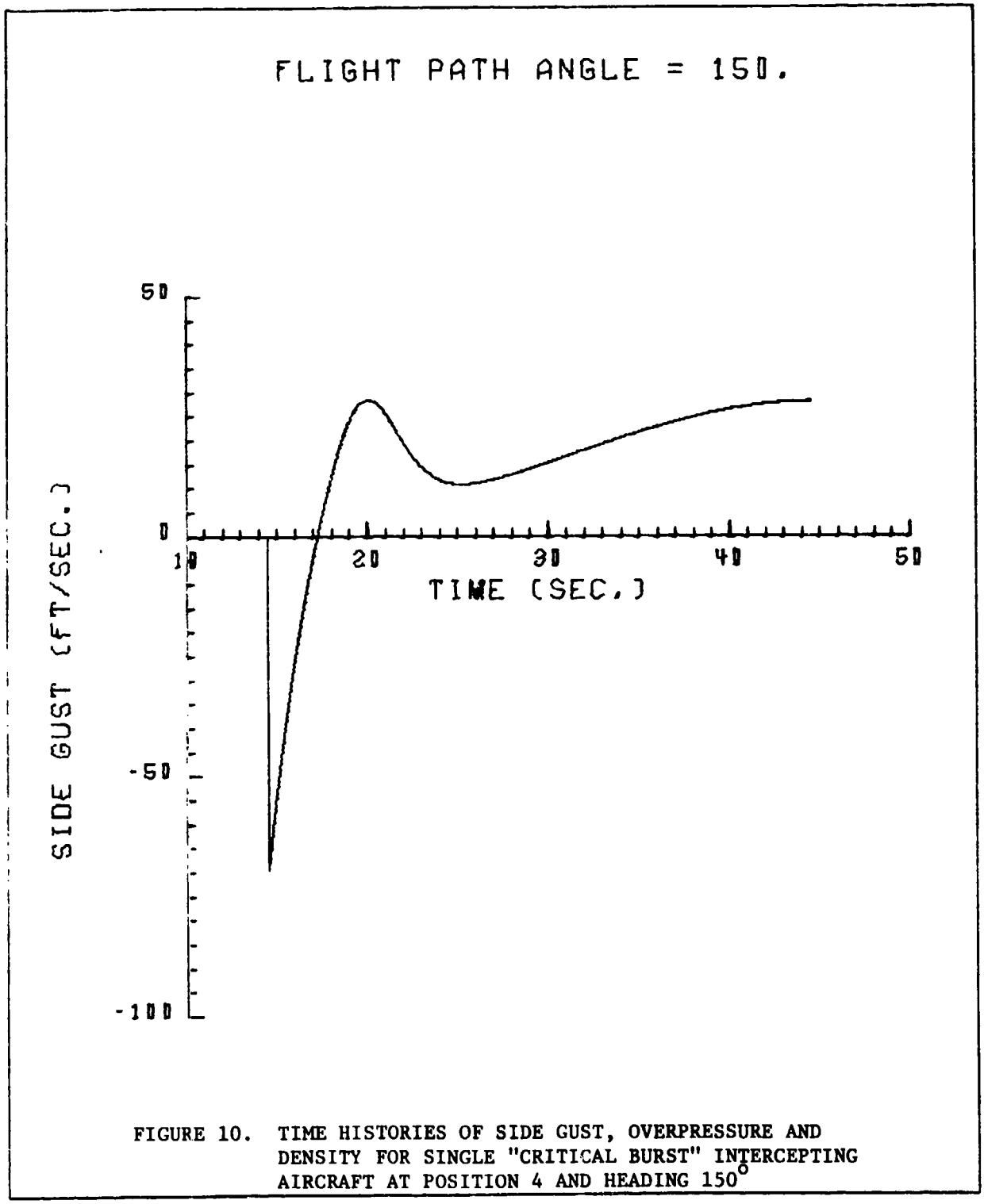

FIGURE 10. TIME HISTORIES OF SIDE GUST, OVERPRESSURE AND DENSITY FOR SINGLE "CRITICAL BURST" INTERCEPTING AIRCRAFT AT POSITION 4 AND HEADING 150°

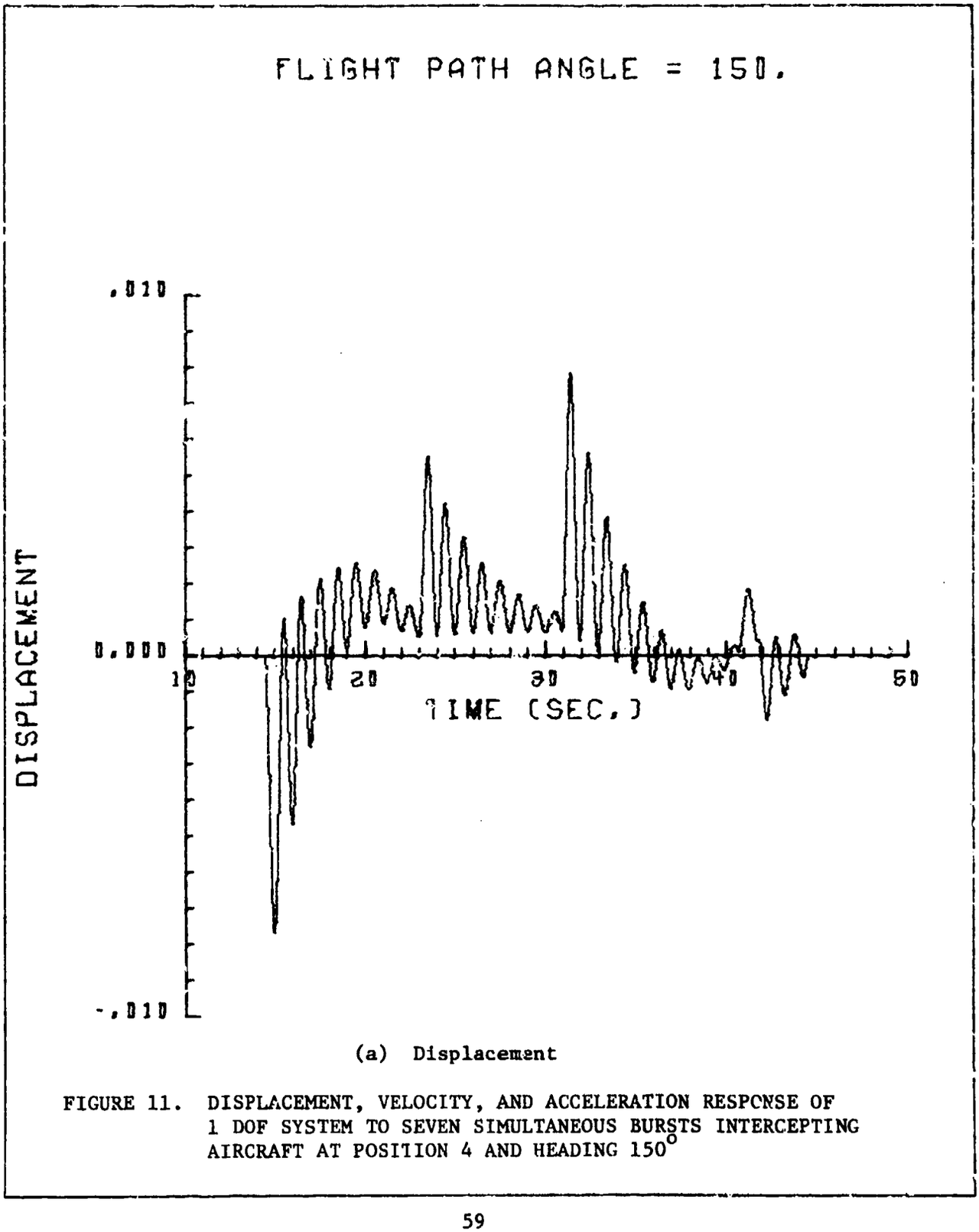

(a) Displacement

FIGURE 11. DISPLACEMENT, VELOCITY, AND ACCELERATION RESPONSE OF 1 DOF SYSTEM TO SEVEN SIMULTANEOUS BURSTS INTERCEPTING AIRCRAFT AT POSITION 4 AND HEADING 150°

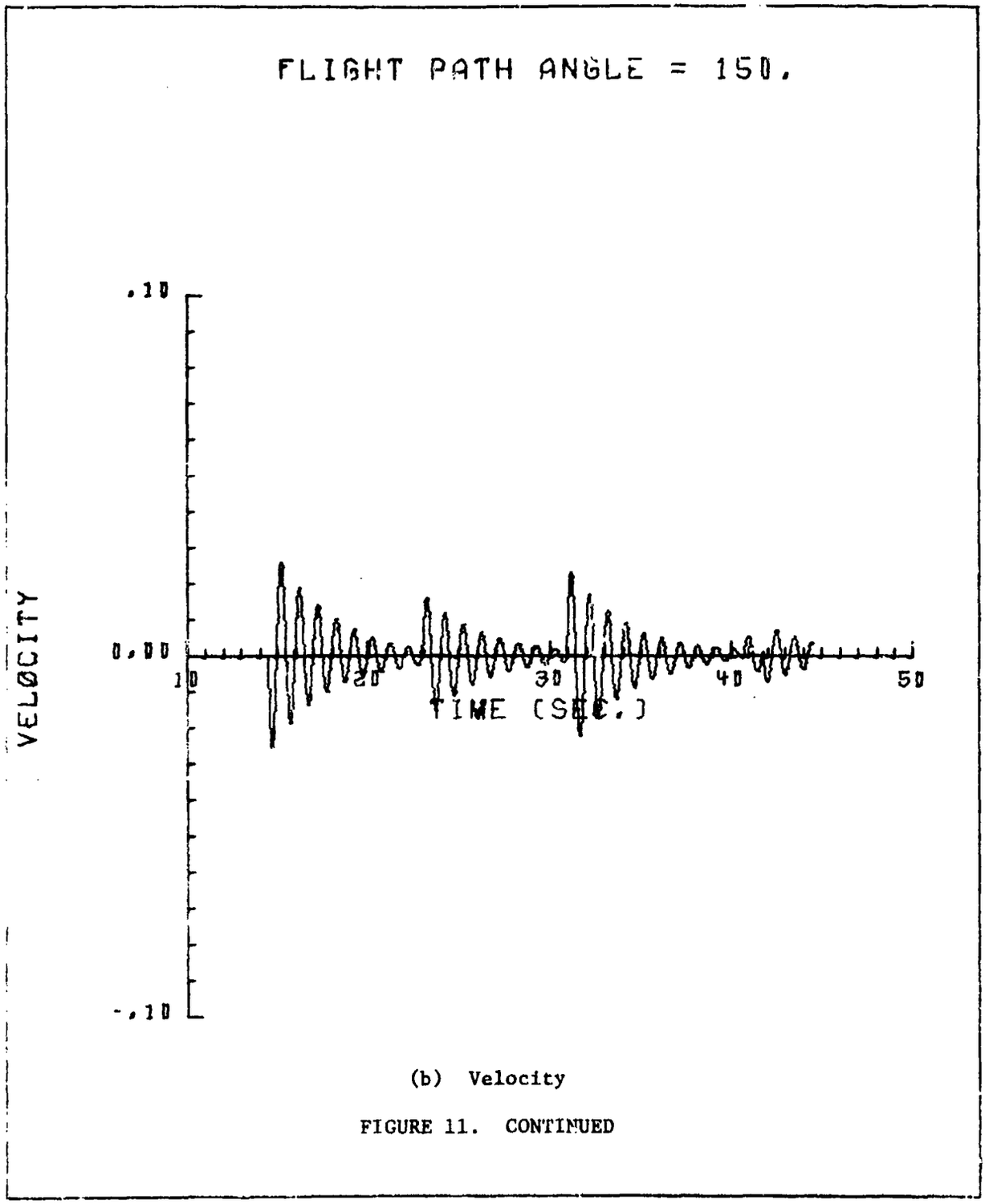

(b) Velocity

FIGURE 11. CONTINUED

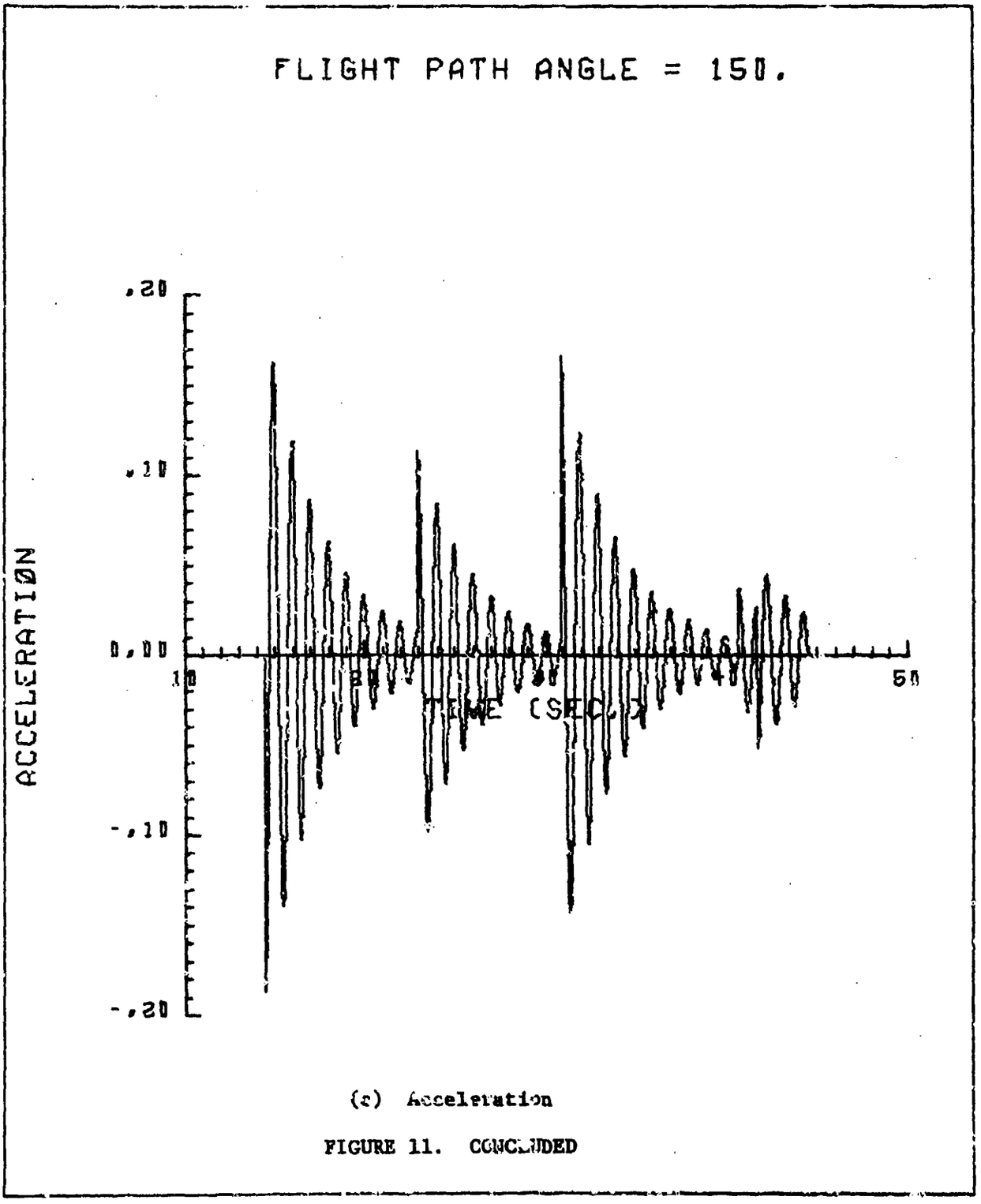

(c) Acceleration

FIGURE 11. CONCLUDED

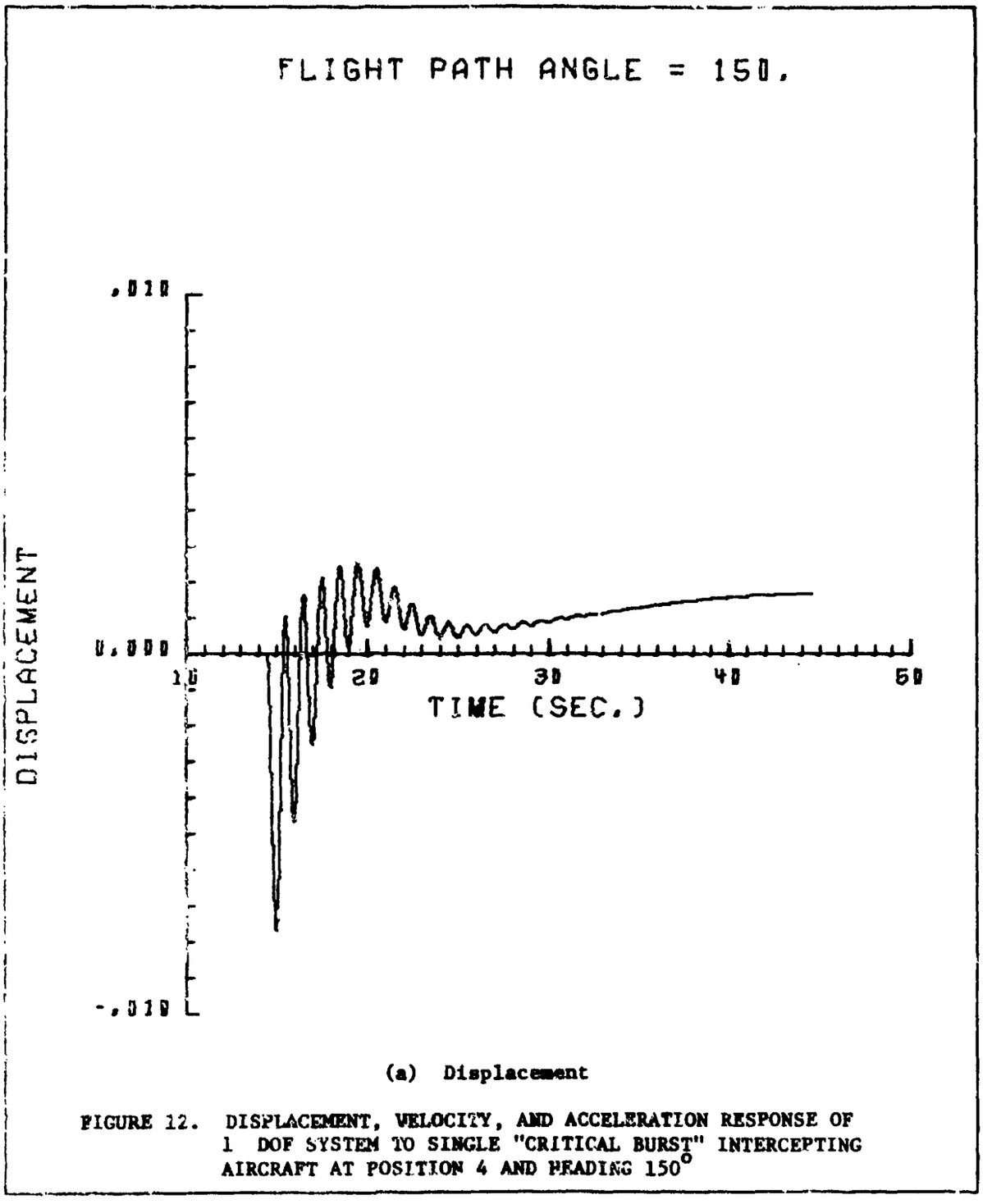

(a) Displacement

FIGURE 12. DISPLACEMENT, VELOCITY, AND ACCELERATION RESPONSE OF 1 DOF SYSTEM TO SINGLE "CRITICAL BURST" INTERCEPTING AIRCRAFT AT POSITION 4 AND HEADING 150°

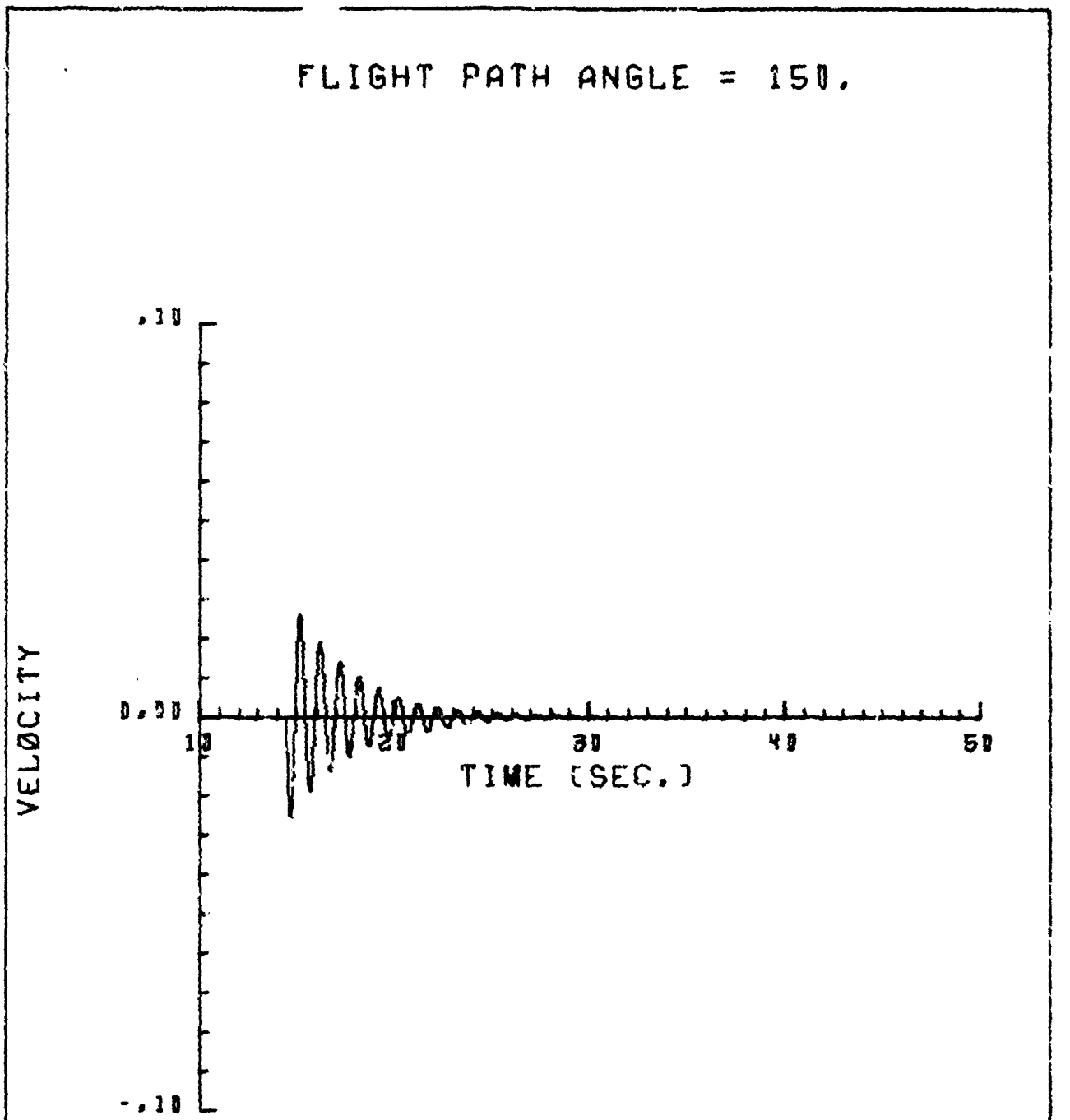

(b) Velocity

FIGURE 12. CONTINUED

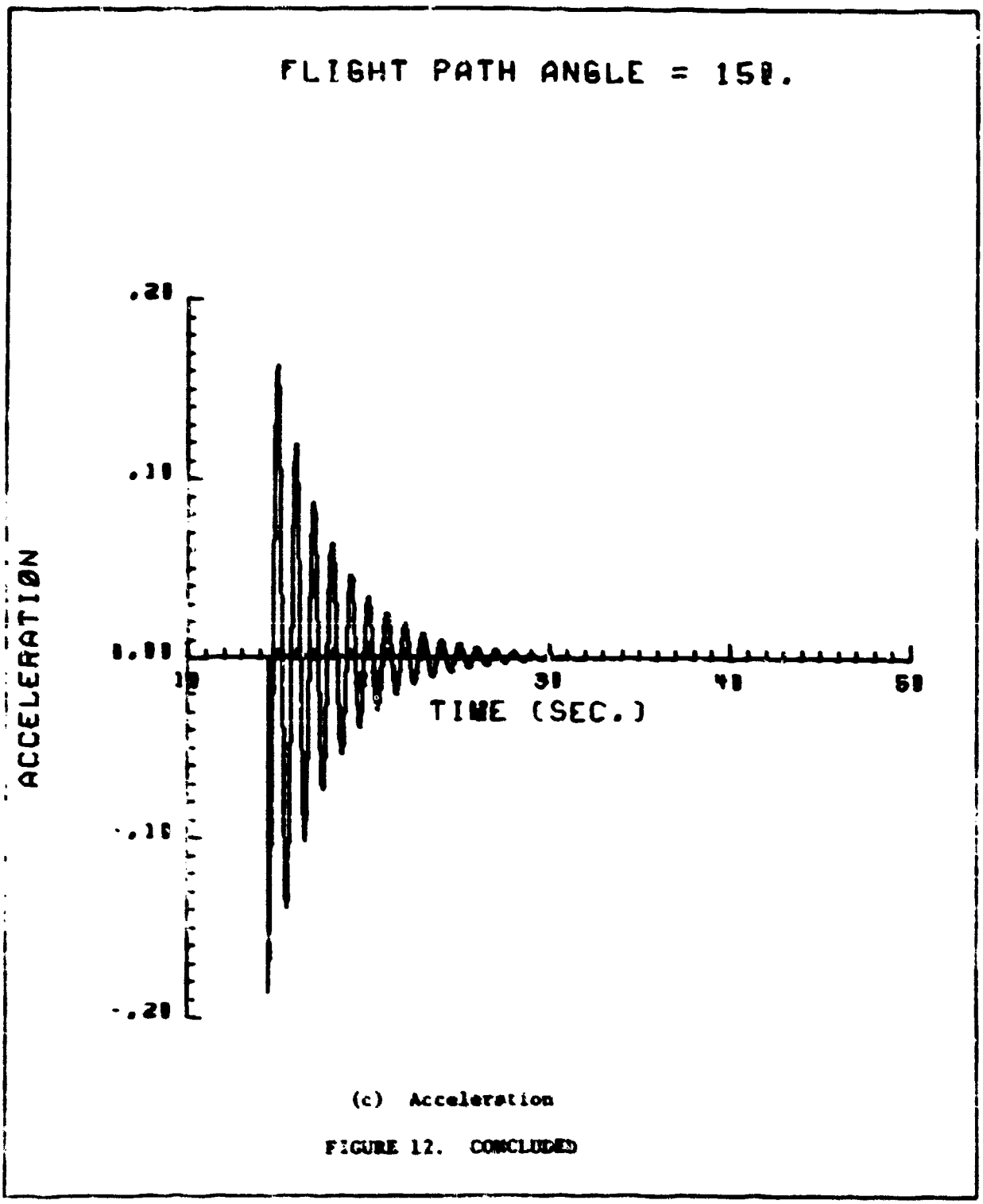

(c) Acceleration

FIGURE 12. CONCLUDED

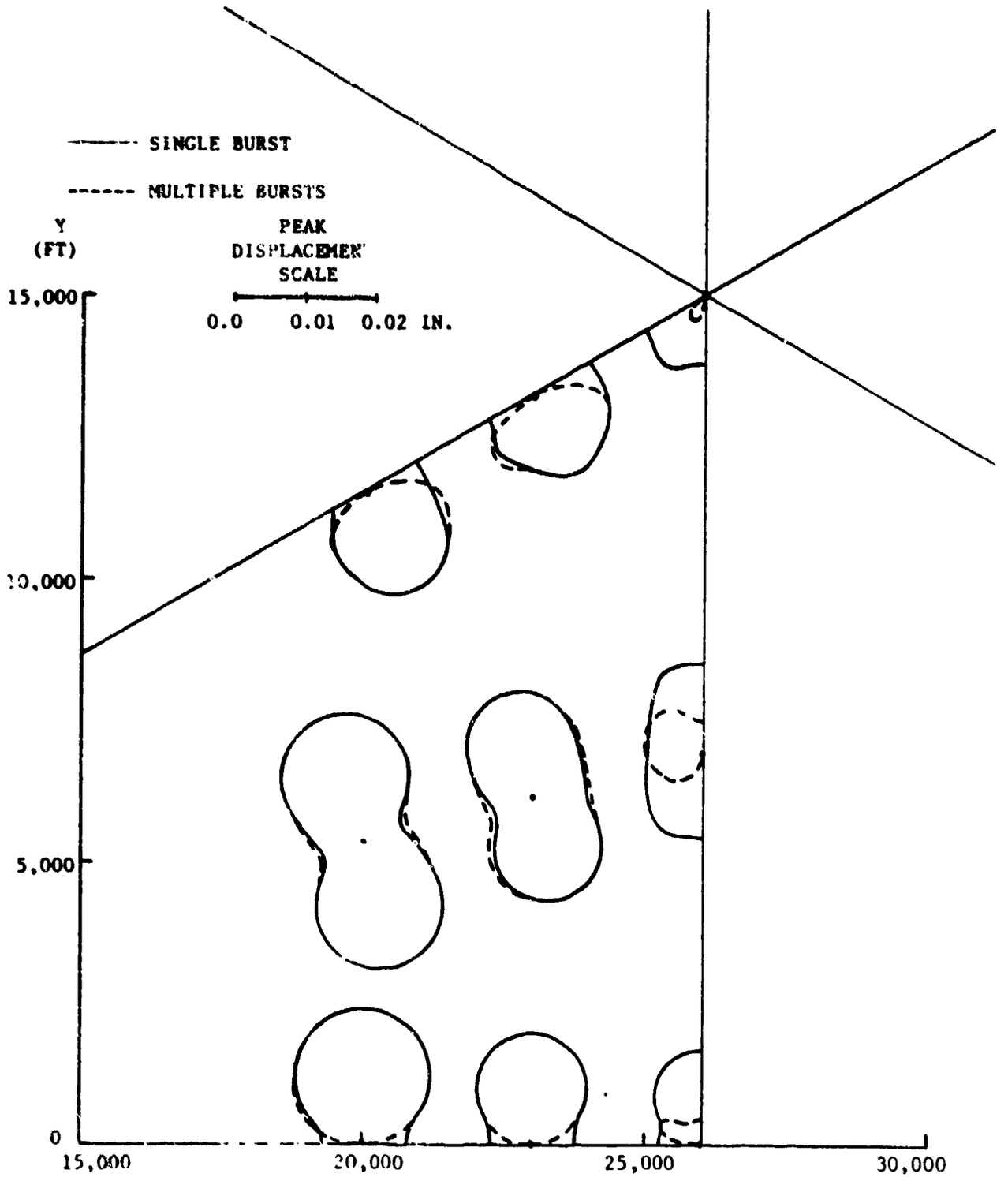

(a) 1 HZ RESPONSE

FIGURE 13. ENVELOPES FOR PEAK DISPLACEMENTS OF 1 DOF SYSTEM SUBJECTED TO GUST LOADING

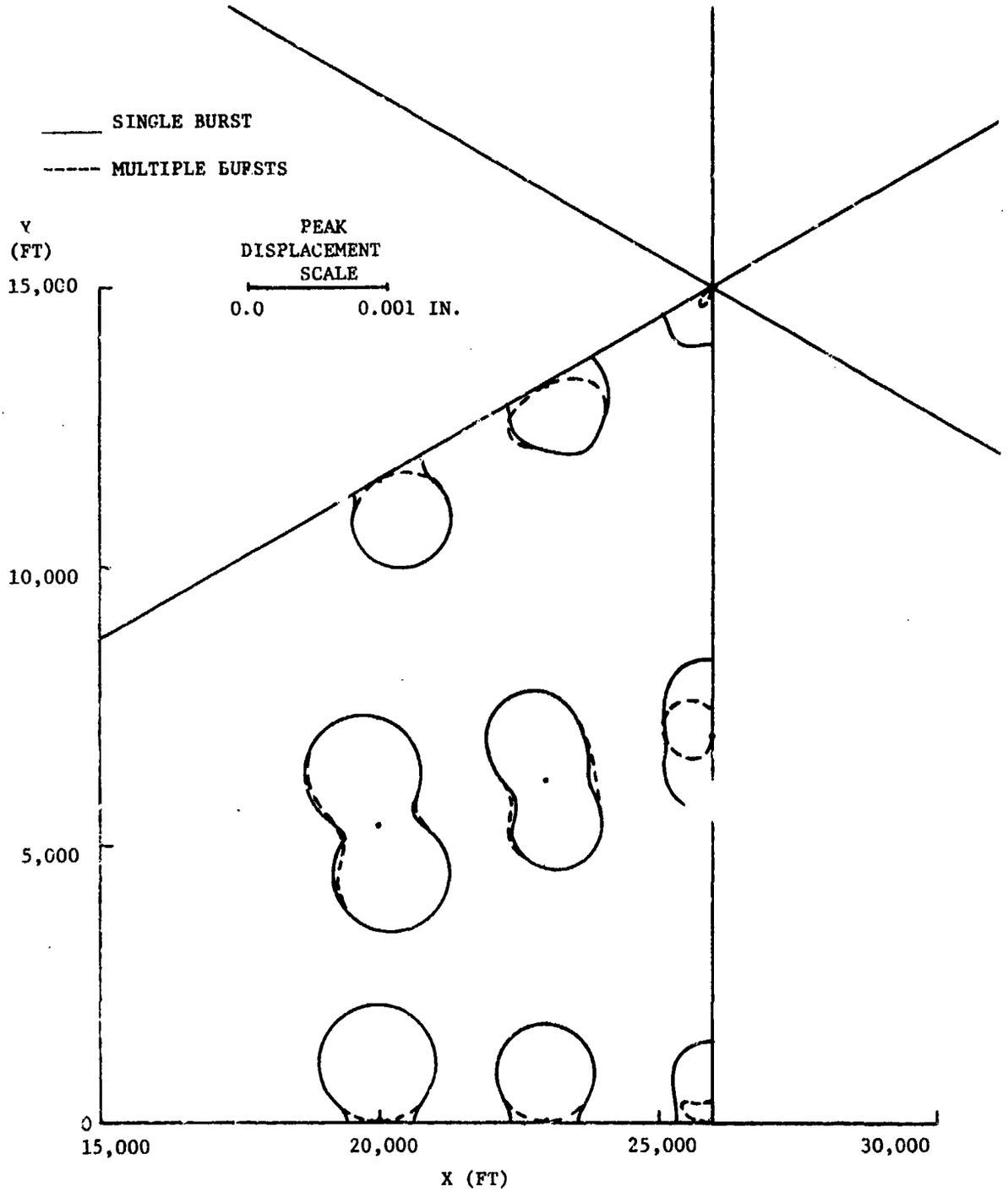

(b) 5 HZ RESPONSE
FIGURE 13. CONCLUDED

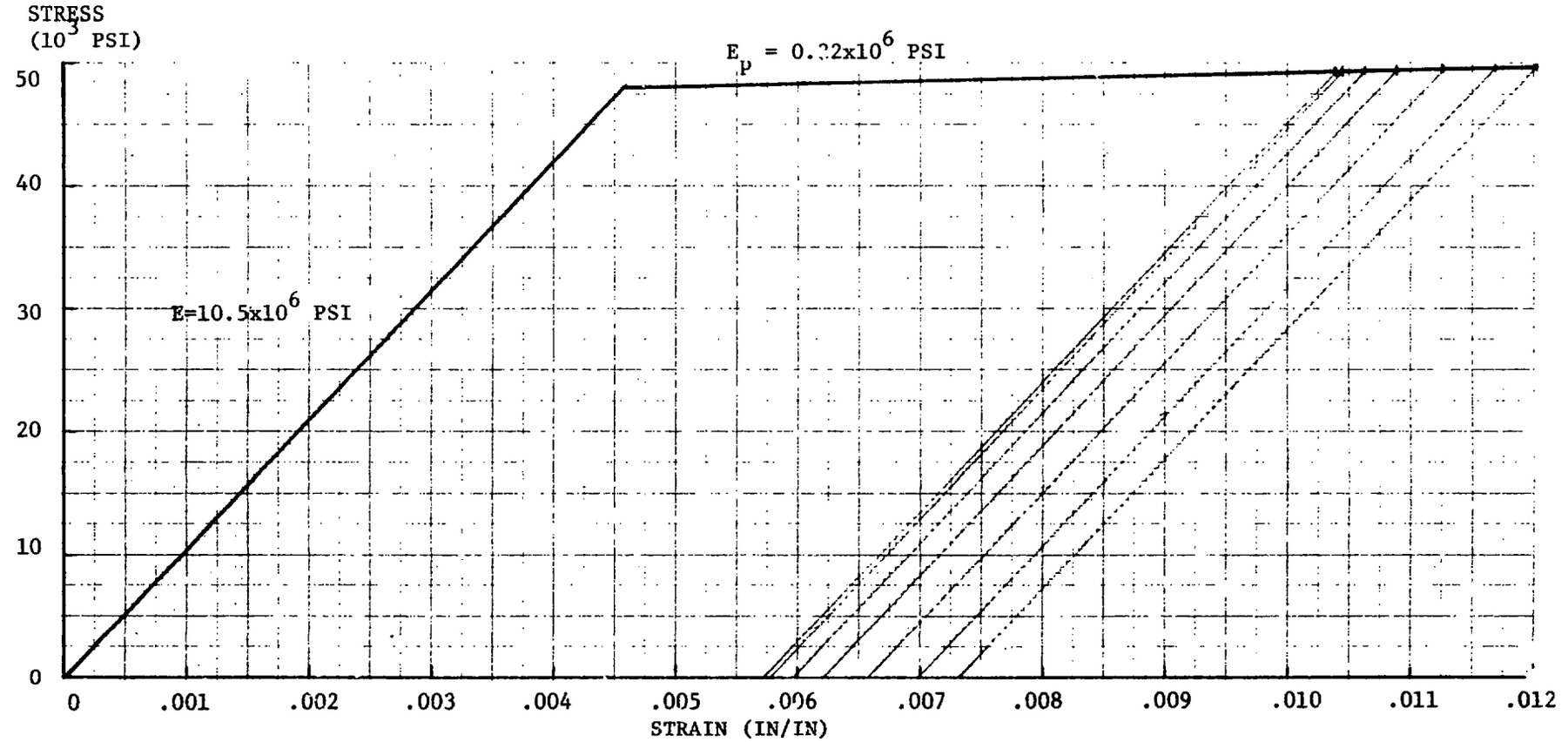

FIGURE 14. STRESS-STRAIN BILINEAR CURVE FOR 2024-T3 ALUMINUM BEAM MODEL, SHOWING STRAIN RECOVERY LINES

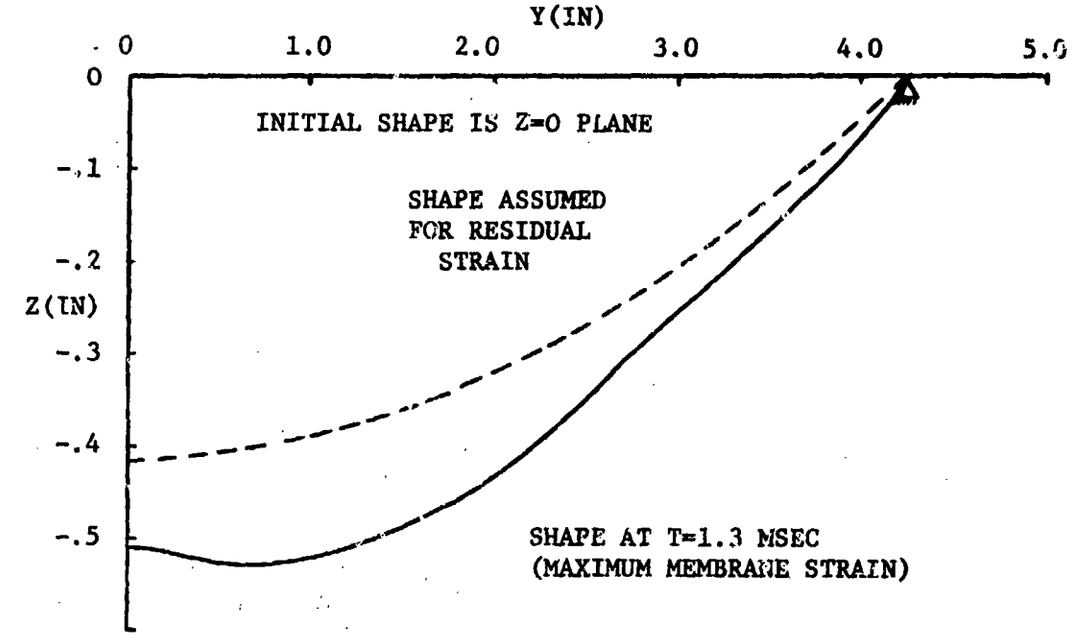

(a) Deformed Beam Shape

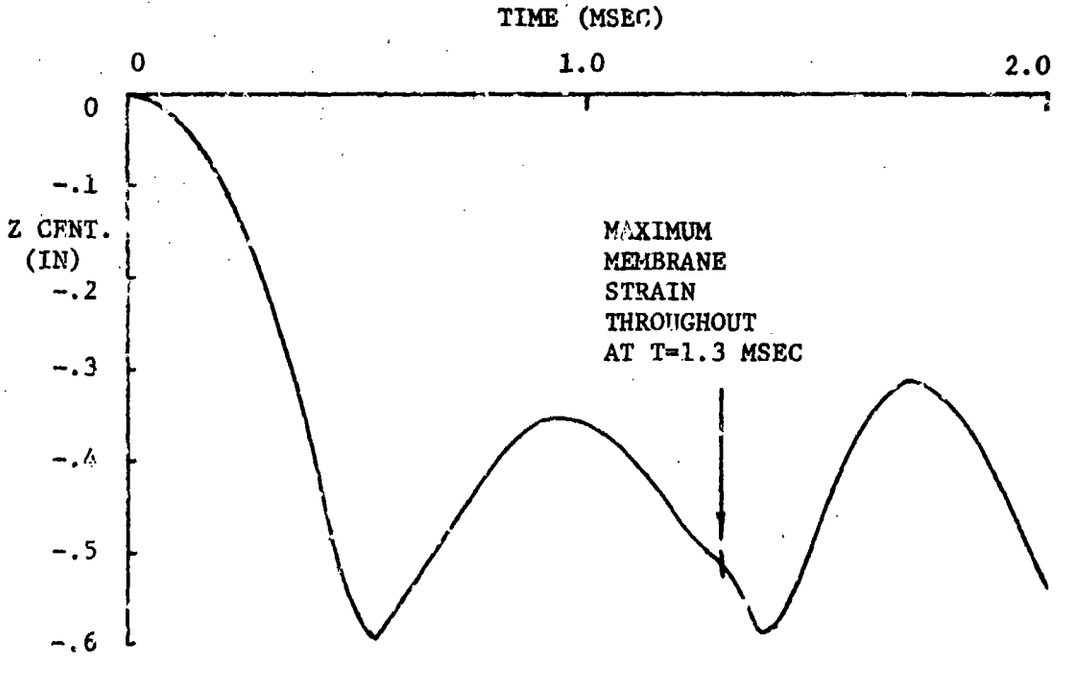

(b) Center Deflection

FIGURE 15. DEFORMED BEAM SHAPE AND CENTER DEFLECTION HISTORY DUE TO FIRST BLAST EXPOSURE

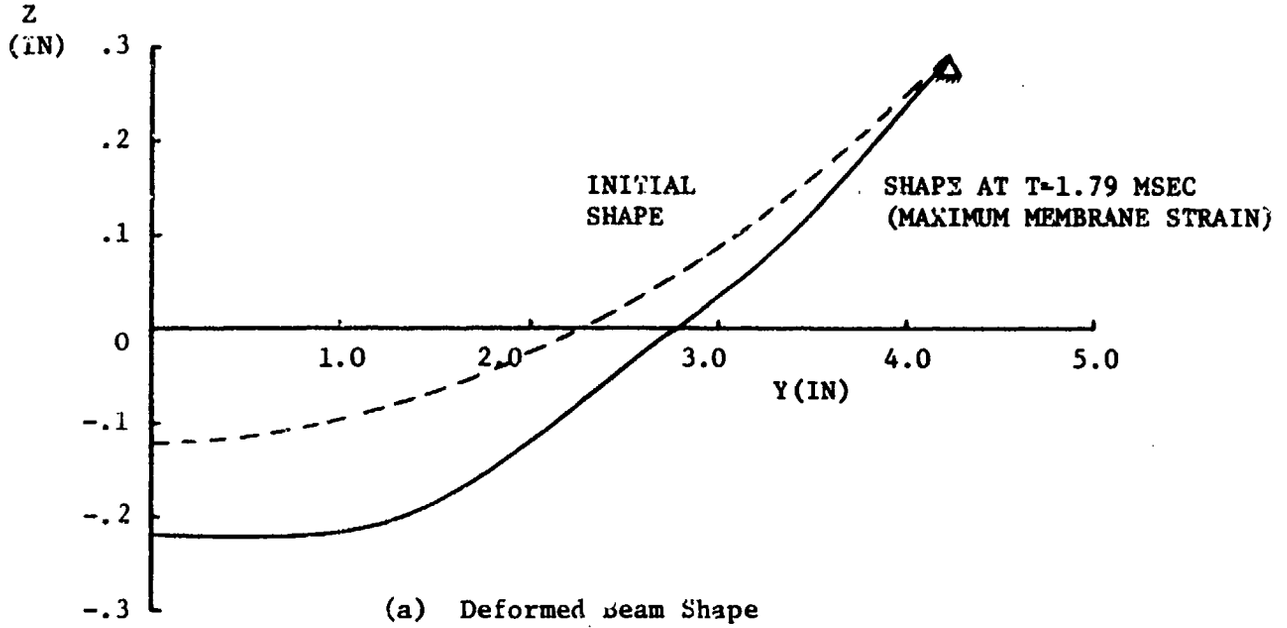

(a) Deformed Beam Shape

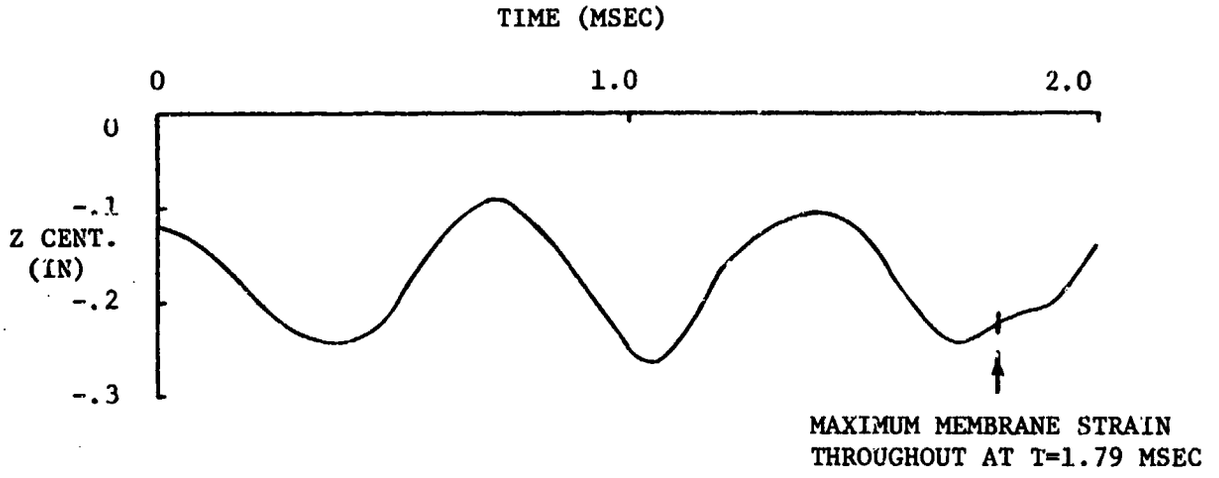

(b) Center Deflection

FIGURE 16. DEFORMED BEAM SHAPE AND CENTER DEFLECTION HISTORY DUE TO SECOND BLAST EXPOSURE

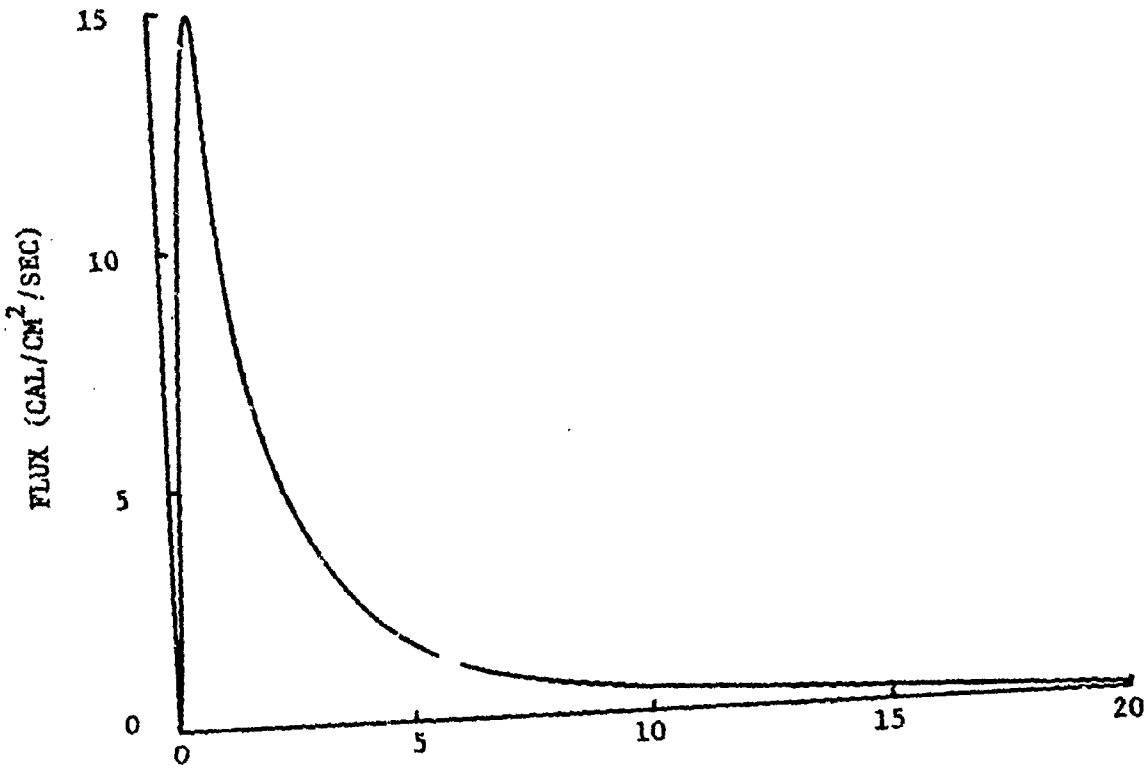

FIGURE 17. INCIDENT THERMAL PULSE AT A RANGE OF 26,000 FEET

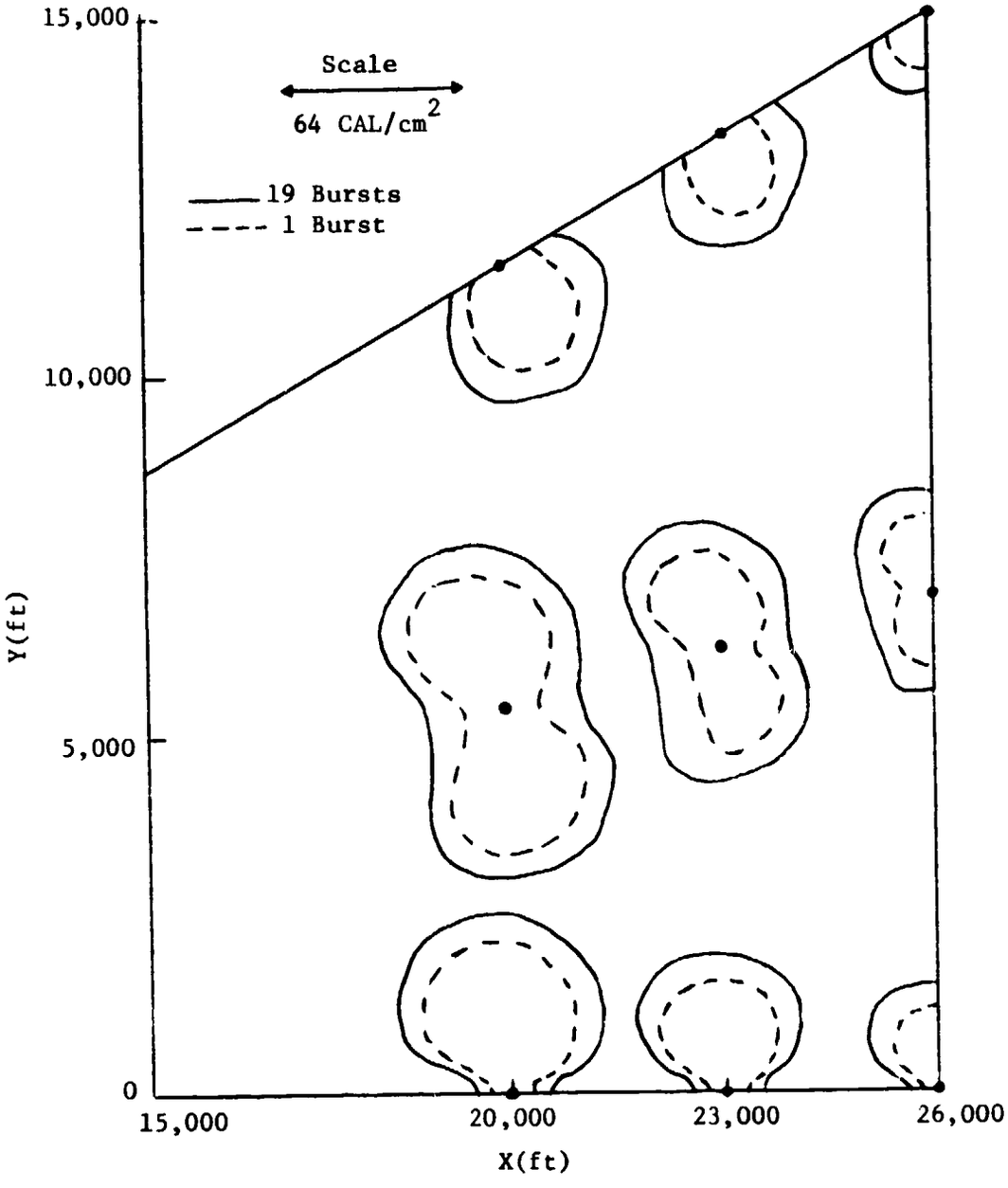

FIGURE 18. INCIDENT THERMAL FLUENCE ENVELOPES FOR SINGLE BURST AND NINETEEN BURST ENVIRONMENTS FOR SIDE-ON EXPOSURE

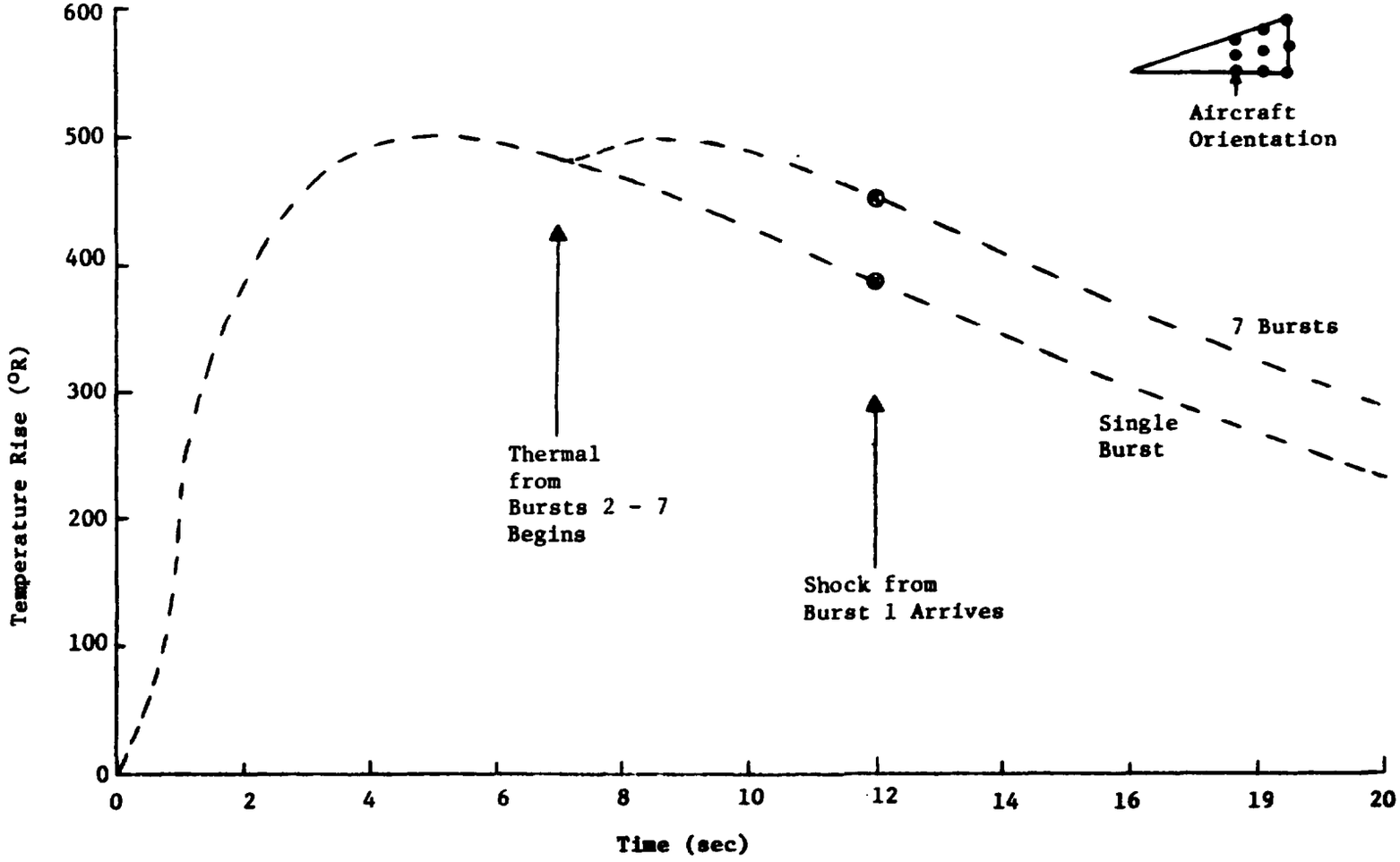

FIGURE 19. SINGLE AND MULTIPLE BURST THERMAL ENVIRONMENT FOR OVERPRESSURE EFFECTS FOR A TYPICAL AIRCRAFT LOCATION

DEPARTMENT OF DEFENSE

Assistant to the Secretary of Defense
Atomic Energy
ATTN: ATSD (AE)

Defense Documentation Center
Cameron Station
12 cy ATTN: TC

Director
Defense Nuclear Agency
ATTN: STSP
ATTN: SPAS
ATTN: TISI
ATTN: DDST
3 cy ATTN: TITL

Commander
Field Command, Defense Nuclear Agency
ATTN: FCPR

Chief
Livermore Division, Fld. Command, DNA
ATTN: FCPRL

Commandant
NATO School (SHAPE)
ATTN: U.S. Documents Officer

Under Sec'y of Def. for Rsch. & Engrg.
ATTN: S&SS (OS)

DEPARTMENT OF THE ARMY

Commander
Harry Diamond Laboratories
ATTN: DELHD-NP
ATTN: DELHD-RBH, J. Gwaltney

Director
U.S. Army Ballistic Research Labs.
ATTN: DRXBR-X, J. Meszaros

Commander
U.S. Army Materiel Dev. & Readiness Cmd.
ATTN: DRCDE-D, L. Flynn

Commander
U.S. Army Nuclear & Chemical Agency
ATTN: Library

DEPARTMENT OF THE NAVY

Chief of Naval Material
ATTN: MAT 0323

Chief of Naval Research
ATTN: Code 464, T. Quinn

Director
Naval Research Laboratory
ATTN: Code 2627

Officer-in-Charge
Naval Surface Weapons Center
ATTN: K. Caudle

DEPARTMENT OF THE NAVY (Continued)

Commanding Officer
Naval Weapons Evaluation Facility
ATTN: P. Hughes

Director
Strategic Systems Project Office
ATTN: NSP-272

DEPARTMENT OF THE AIR FORCE

AF Materials Laboratory, AFSC
ATTN: MBC, D. Schmidt
ATTN: MBE, G. Schmitt

AF Weapons Laboratory, AFSC
ATTN: DYV, A. Sharp
ATTN: SUL

Commander
ASD
4 cy ATTN: ENFTV, D. Ward

Commander
Foreign Technology Division, AFSC
ATTN: PDBF, Mr. Spring

Commander in Chief
Strategic Air Command
ATTN: XPFS

DEPARTMENT OF ENERGY

Sandia Laboratories
ATTN: Doc. Con. for Dept. 1310, A. Lieber

DEPARTMENT OF DEFENSE CONTRACTORS

Aerospace Corp.
ATTN: W. Barry

Avco Research & Systems Group
ATTN: W. Broding
ATTN: J. Patrick

Boeing Co.
ATTN: E. York
ATTN: R. Dyrdahl

Boeing Wichita Co.
ATTN: R. Syring
ATTN: D. Pierson

Effects Technology, Inc.
ATTN: R. Parisse

General Dynamics Corp.
Pomona Division
ATTN: R. Shemensky

General Electric Co.-TEMPO
Center for Advanced Studies
ATTN: DASIAC

Kaman Sciences Corp.
ATTN: D. Sachs

DISTRIBUTION LIST

DEPARTMENT OF DEFENSE CONTRACTORS (Continued)

Kaman AviDyne
Division of Kaman Sciences Corp.
ATTN: N. Hobbs
ATTN: R. Yeghiayan
ATTN: W. Lee
ATTN: J. Walsh

Martin Marietta Corp.
Orlando Division
ATTN: G. Aiello

McDonnell Douglas Corp.
ATTN: J. McGrew

Northrop Corp.
ATTN: D. Hicks

DEPARTMENT OF DEFENSE CONTRACTORS (Continued)

Prototype Development Associates, Inc.
ATTN: J. McDonald

R & D Associates
ATTN: J. Carpenter
ATTN: A. Latter
ATTN: F. Field

Rockwell International Corp.
ATTN: R. Sparling

Science Applications, Inc.
ATTN: D. Hove

SRI International
ATTN: G. Abrahamson